Report

Cell Reports

Huntingtin Inclusions Trigger Cellular Quiescence, Deactivate Apoptosis, and Lead to Delayed Necrosis

Graphical Abstract

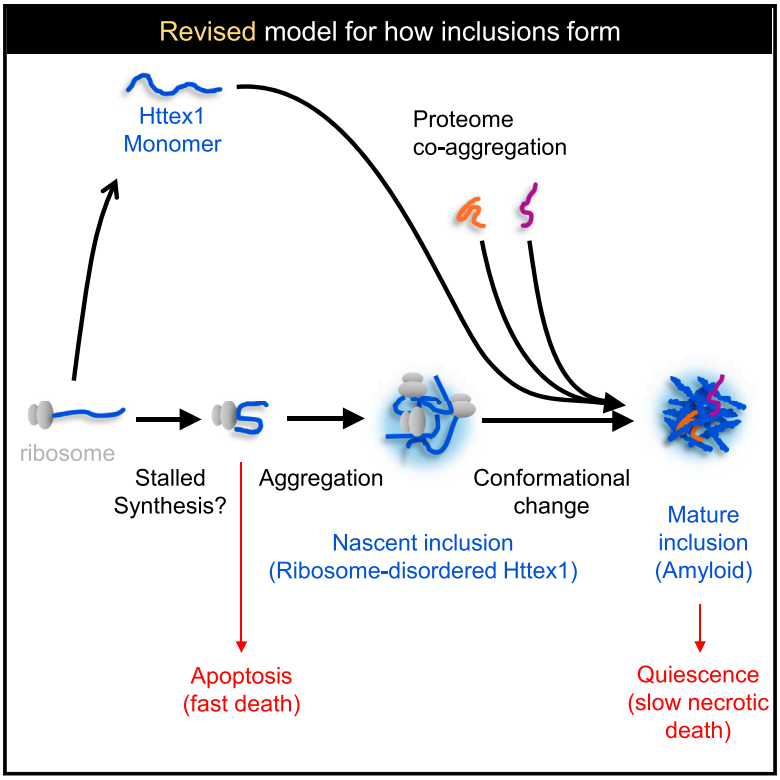

Authors

Yasmin M. Ramdzan, Mikhail M. Trubetskov, Angelique R. Ormsby, ..., David B. Ascher, Gavin E. Reid, Danny M. Hatters

Correspondence

dhatters@unimelb.edu.au

In Brief

Httex1 aggregation into inclusions has paradoxically been reported as either toxic or beneficial in Huntington's disease. Ramdzan et al. define a dual mechanism of toxicity that explains this paradox. Soluble Httex1 triggers a fast death by apoptosis, whereas Httex1 inclusions invoke quiescence and redirect death to a slower necrotic pathway.

Highlights

- Soluble mutant Huntingtin exon 1 (Httex1) triggers apoptosis
- Httex1 inclusions deactivate apoptosis but activate delayed necrosis
- Nascent inclusions form from disordered Httex1 and ribosomes
- Upon maturation, Httex1 converts into amyloid and co-recruits prion domain proteins

Accession Numbers

PXD005120

Ramdzan et al., 2017, Cell Reports *19*, 919–927
May 2, 2017
http://dx.doi.org/10.1016/j.celrep.2017.04.029

Cell Reports
Report

Huntingtin Inclusions Trigger Cellular Quiescence, Deactivate Apoptosis, and Lead to Delayed Necrosis

Yasmin M. Ramdzan,[1,14] Mikhail M. Trubetskov,[1,14] Angelique R. Ormsby,[1] Estella A. Newcombe,[1] Xiaojing Sui,[1] Mark J. Tobin,[2] Marie N. Bongiovanni,[3] Sally L. Gras,[4] Grant Dewson,[5,6] Jason M.L. Miller,[7] Steven Finkbeiner,[8] Nagaraj S. Moily,[1] Jonathan Niclis,[9] Clare L. Parish,[9] Anthony W. Purcell,[10] Michael J. Baker,[1] Jacqueline A. Wilce,[10] Saboora Waris,[10] Diana Stojanovski,[1] Till Böcking,[11] Ching-Seng Ang,[12] David B. Ascher,[1] Gavin E. Reid,[1,13] and Danny M. Hatters[1,15,*]

[1]Department of Biochemistry and Molecular Biology and Bio21 Molecular Science and Biotechnology Institute, The University of Melbourne, Melbourne, VIC 3010, Australia
[2]Australian Synchrotron, 800 Blackburn Road, Clayton, VIC 3168, Australia
[3]Department of Chemistry, University of Cambridge, Cambridge CB2 1EW, UK
[4]Department of Chemical and Biomolecular Engineering and Bio21 Molecular Science and Biotechnology Institute, The University of Melbourne, Melbourne, VIC 3010, Australia
[5]Walter and Eliza Hall Institute of Medical Research, 1G Royal Parade, Parkville, VIC 3052, Australia
[6]Department of Medical Biology, University of Melbourne, Parkville, Melbourne, VIC 3010, Australia
[7]University of Michigan Kellogg Eye Center, 1000 Wall Street, Ann Arbor, MI 48105, USA
[8]Gladstone Institute of Neurological Disease, 1650 Owens Street, San Francisco, CA 94158-2261, USA
[9]The Florey Institute of Neuroscience and Mental Health, The University of Melbourne, Parkville, VIC 3010, Australia
[10]Monash Biomedicine Discovery Institute and Department of Biochemistry and Molecular Biology, Monash University, Clayton, VIC 3800, Australia
[11]School of Medical Sciences, The University of New South Wales, Sydney, NSW 2052, Australia
[12]Bio21 Mass Spectrometry and Proteomics Facility, The University of Melbourne, Melbourne, VIC 3010, Australia
[13]School of Chemistry, The University of Melbourne, Melbourne, VIC 3010, Australia
[14]These authors contributed equally
[15]Lead Contact
*Correspondence: dhatters@unimelb.edu.au
http://dx.doi.org/10.1016/j.celrep.2017.04.029

SUMMARY

Competing models exist in the literature for the relationship between mutant Huntingtin exon 1 (Httex1) inclusion formation and toxicity. In one, inclusions are adaptive by sequestering the proteotoxicity of soluble Httex1. In the other, inclusions compromise cellular activity as a result of proteome co-aggregation. Using a biosensor of Httex1 conformation in mammalian cell models, we discovered a mechanism that reconciles these competing models. Newly formed inclusions were composed of disordered Httex1 and ribonucleoproteins. As inclusions matured, Httex1 reconfigured into amyloid, and other glutamine-rich and prion domain-containing proteins were recruited. Soluble Httex1 caused a hyperpolarized mitochondrial membrane potential, increased reactive oxygen species, and promoted apoptosis. Inclusion formation triggered a collapsed mitochondrial potential, cellular quiescence, and deactivated apoptosis. We propose a revised model where sequestration of soluble Httex1 inclusions can remove the trigger for apoptosis but also co-aggregate other proteins, which curtails cellular metabolism and leads to a slow death by necrosis.

INTRODUCTION

Huntington's disease (HD) is caused by dominant CAG trinucleotide expansion mutations in the *HTT* gene (MacDonald et al., 1993). These mutations encode an abnormally long polyglutamine (polyQ) sequence in the Huntingtin (Htt) protein, which causes its aggregation into amyloid-like fibrils (Scherzinger et al., 1999). Aggregation of N-terminal Htt fragments into intracellular inclusions is one of the key molecular signatures of HD (DiFiglia et al., 1997; Scherzinger et al., 1997). Despite this, the role of aggregation in toxicity is unclear. Aggregates, in particular soluble oligomers, have been reported to be proteotoxic (Lajoie and Snapp, 2010; Leitman et al., 2013; Nucifora et al., 2012; Takahashi et al., 2008). Aggregates may also be toxic by sequestration of critical factors required for normal growth and viability, such as transcription factors (Schaffar et al., 2004), chaperones (Park et al., 2013), and nuclear-cytoplasmic transport machinery (Woerner et al., 2016). Inclusions may also arise from (or cause) a more general collapse of proteostasis (Gidalevitz et al., 2006).

Seemingly paradoxical to the hypothesis that aggregation correlates with toxicity are data showing that formation of inclusions improves survival odds (Arrasate et al., 2004; Bodner et al., 2006). This has led to the alternative hypothesis that inclusions are formed to sequester dispersed low-oligomeric states of Httex1 and, hence, protect the cell from their harmful effects. However, the mechanisms that can reconcile the observations underpinning these two seemingly contrasting hypotheses remain unknown.

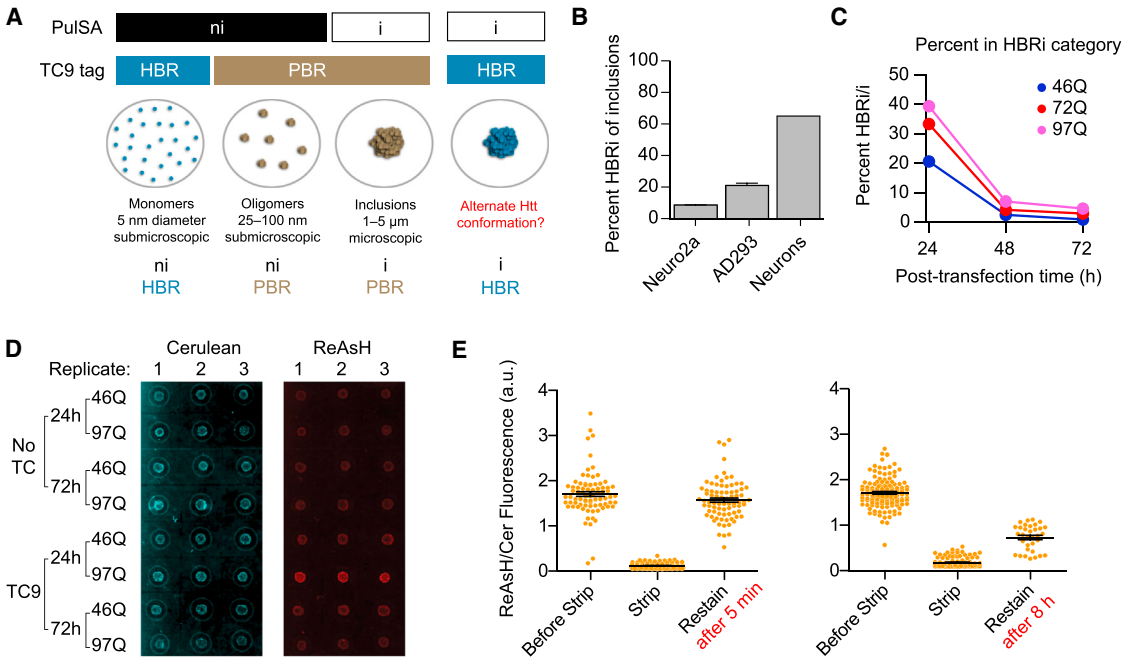

Figure 1. Formation of the HBRi and PBRi Subclasses

(A) Flow cytometry gating strategy. Collective classification of HBR and i denote an unexpected population in the cell.

(B) Formation of HBRi in three different cell types expressing Httex1^{TC9}(97Q)-Cerulean as assessed by confocal imaging. Cortical neurons were differentiated from human embryonic stem cells and stained for ReAsH 5 days after lentiviral transduction of the construct. Neuro2a and AD293 cells were stained 24 hr post-transfection.

(C) Formation of the HBRi class of inclusions in AD293 cells transfected with Httex1^{TC9}-Cerulean of the indicated polyQ lengths, measured by flow cytometry.

(D) Native slot blots of insoluble fractions of Neuro2a cell lysates harvested at the indicated time points after transfection and after ReAsH staining.

(E) Inclusions lose biarsenical reactivity over time. Plated AD293 cells were stained with ReAsH 24 hr after transfection with Httex1^{TC9}(97Q)-Cerulean and stripped of ReAsH with BAL treatment. Cells were restained with ReAsH after culturing for a further 5 min or 8 hr.

Means and SEM are shown.

Using a biosensor of the Httex1 conformational state, we unearthed two types of inclusions that earmark early and late stages of the inclusion-building process. Investigation of how these inclusions form and relate to the broader homeostatic state of the cell led us to find that inclusion assembly deactivated a heightened risk of apoptosis triggered by soluble mutant Httex1 but, in doing so, initiated a cellular quiescence that led to a slower death by necrosis.

RESULTS

Detection of Early-Formed and Late-Formed Subclasses of Inclusions Formed by Htt Exon 1: HBRi and PBRi

We previously created a biosensor derivative of Httex1, Httex1^{TC9}, that reported on whether the protein was monomeric or in an amyloid conformation through a two-color fluorescence detection scheme (Ramdzan et al., 2010). Conformation was read out by reactivity of engineered tetracysteine tags to the biarsenical dyes 4,6-*bis*(1,3,2-dithiarsolan-2-yl)-7-hydroxy-3H-phenoxazin-3-one (ReAsH) or 4',5'-*bis*(1,3,2-dithiarsolan-2-yl)-3',6'-dihydroxy-spiro[isobenzofuran-1(3H),9'-[9H]xanthen]-3-one (FlAsH), which efficiently bind to the biosensor (highly biarsenically reactive [HBR]) when the tag is accessible in the monomeric, disordered state but do not bind (poorly biarsenically reactive [PBR]) when it is inaccessible in the β sheet-rich amyloid fibril state (Ramdzan et al., 2010). Protein localization was tracked by a Cerulean fluorescent protein tag as the second color channel. We also devised a protocol to rapidly screen cells for localization of the Cerulean tag by a flow cytometry method (pulse shape analysis [PulSA]), which distinguishes cells with inclusions (i) from those with only diffuse Httex1 (no inclusions, ni) (Ramdzan et al., 2012). The use of the biosensor and PulSA together enabled us to distinguish three key groups of cells: cells enriched with Httex1^{TC9} monomers (HBRni), oligomers (PBRni), or inclusions (PBRi) (Figure 1A).

The Httex1^{TC9} biosensor was originally developed using polyQ lengths of 25Q (non-aggregating) or 46Q (aggregating) and applied in the Neuro2a cell line (Ramdzan et al., 2012). When we examined Httex1^{TC9} in other cell lines and with longer polyQ lengths, some of the cells with inclusions displayed high biarsenical reactivity, which we designated as the HBRi population (Figure 1B; see Figures S1A and S1B for further details on expression levels and aggregation extent). The proportion of HBRi cells in cells with inclusions decreased with time, suggesting that biarsenical reactivity is a transient property of cells with inclusions (Figure 1C). Native slot blots of the insoluble fraction

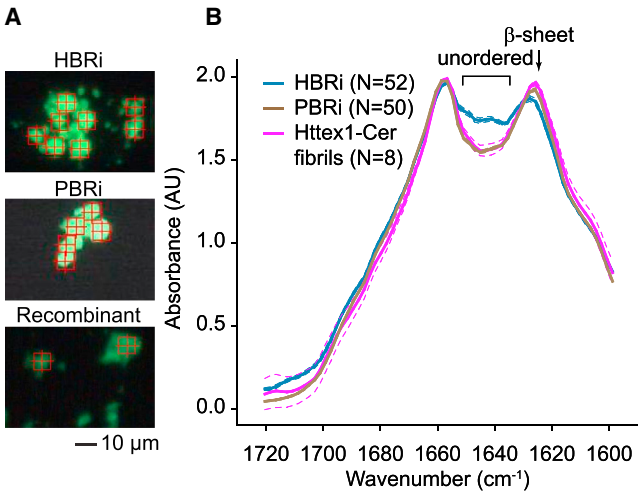

Figure 2. Httex1 Is Disordered in Early-Formed Inclusions and Converts to Amyloid over Time

(A) Fluorescence micrograph of inclusions and amyloid fibrils formed by purified Httex1-Cerulean for FTIR analysis (red cross-hairs mark representative beam clipping windows).

(B) Mean FTIR spectra with replicates referring to individual inclusions. Solid lines show means, and dashed lines show SEM.

of whole-cell lysate labeled with ReAsH at different time points after transfection supported this conclusion (Figure 1D). In addition, HBRi-categorized cells were proportionally more abundant at lower expression levels (Figure S1C) and had smaller inclusions (Figure S1D).

These data suggested that HBRi status earmarked an earlier step in the inclusion assembly process and PBRi a more mature state. To test this hypothesis, we examined the capacity of HBRi cells to be restained with ReAsH over time. Inclusions could be stripped with ReAsH using a non-toxic reducing agent (British anti-Lewisite [BAL]) and fully restained after 5 min (Figure 1E). However, staining after 8 hr led to a significant reduction in reactivity, consistent with a conversion to PBRi status (Figure 1E).

For clues to why Httex1 adopts an aggregated state permissive to biarsenical reactivity in HBRi inclusions, we examined the protein secondary structure of purified individual inclusions using synchrotron Fourier transform infrared (FTIR) microscopy (Figure 2A; Figures S2A and S2B). The amide I spectra of inclusions of the PBRi category on average matched those of recombinant Httex1-Cerulean amyloid fibrils, consistent with a notable β sheet signal (~1626 cm^{-1}) (Figure 2B; Figure S3A). By contrast, HBRi-categorized inclusions on average substantially differed to PBRi with less β sheet and greater disordered structure (Figure 2B; Figure S3A). The HBRis were also more heterogeneous than PBRi inclusions (Figure S3A). Multivariate analysis indicated that HBRis formed a continuum of states that, on one end, consisted of disordered structure and, on the other end, were more similar to the PBRi state (Figure S3B). These data suggested that biarsenical reactivity in the HBRi state arises from the accumulation of non-amyloid disordered structure, whereby the tetracysteine tag remains solvent-accessible (in contrast to the amyloid conformation).

Inclusion Formation Suppresses Apoptosis and Leads to a Delayed Necrosis

During our time-lapse imaging analysis, we noticed that just over half of the cells labeled as PBRi at 24 hr died non-apoptotically, whereas those retaining diffuse Httex1 or earmarked as HBRi (at 24 hr) died almost entirely by apoptosis (Figure 3A; details on how we classified the cells by microscopy are shown in Figure S4). This result led us to speculate that inclusion formation deactivated a risk of apoptosis arising from the soluble Httex1 forms.

To test this hypothesis, we first applied a broad-spectrum caspase inhibitor, (3S)-5-(2,6-Difluorophenoxy)-3-[[(2S)-3-methyl-1-oxo-2-[(2-quinolinylcarbonyl)amino]butyl]amino]-4-oxo-pentanoic acid hydrate (QVD-OPh) (Caserta et al., 2003), which both abrogated the apoptotic death (Figure 3A) and substantially increased the survival time of all cell groups (Figure 3B). We also found that when cells formed an inclusion, death by apoptosis was significantly correlated to shorter survival times than cells that died by necrosis (Figure 3C; these effects were not correlated with the expression level; Figure S5). We fitted the data in Figures 3A–3C to a simple three-state model to define the relative risks of apoptosis as inclusions form and mature. This yielded an excellent fit (correlation coefficient of 0.96) and indicated risks of apoptosis 4.8-fold higher for cells retaining soluble Httex1 versus HBRi and 8-fold higher for cells retaining soluble Httex1 versus PBRi (Figure 3D; full details of the fit can be found in Table S1).

To examine whether the origin for risk of apoptosis resided in the pool of soluble Httex1, we measured the levels of diffuse Httex1 in cells both at the time point of HBRi and PBRi classification (24 hr; Figure 3E) as well as 1 hr prior to death (Figure 3F). In both cases, the levels of soluble Httex1 were higher in cells with HBRi and in cells that die by apoptosis.

Next we developed an independent method to track early-formed inclusions and late-formed inclusions to investigate the possibility that apoptosis is triggered as an artifact of the biarsenical dyes. This involved fusing Httex1 to the fluorescent timer (FT)-fast protein, which converts blue to red fluorescence over a period of several hours (Subach et al., 2009). As inclusions formed and trapped Httex1 proteins, cells containing inclusions became progressively more red-fluorescent over time; hence, the "color" of the cells with inclusions, as measured with PulSA (or microscopy), enabled a distinction of cells with "young" inclusions from those with "old" inclusions (Figures S6A and 6B). This strategy to classify inclusions at 24 hr of expression (by microscopy) resulted in similar patterns for survival and mechanisms of death to that determined with the biarsenical dye strategy, indicating that the biarsenical dyes do not aberrantly induce apoptosis (Figures S6C and 6D).

Using the timer protein approach, we also tested whether cells with old inclusions were functionally impaired from activating apoptosis. Three pharmacological stimulants of apoptosis were able to activate apoptosis in cells with old inclusions (Figure S6D). Hence, we concluded that inclusion formation disarms

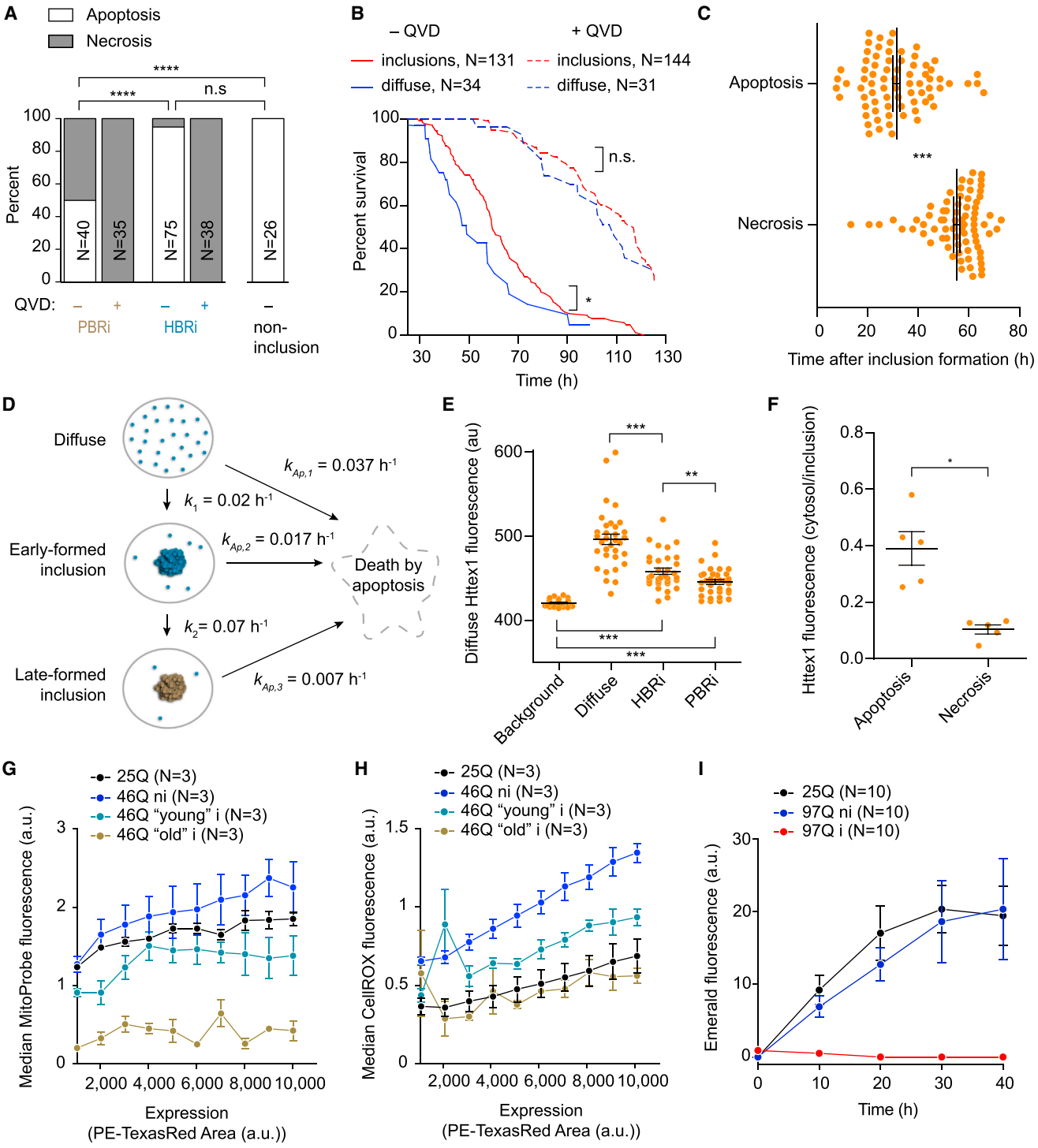

Figure 3. Inclusion Formation Disables Apoptosis, Promotes Quiescence, and Switches Death to Slow Necrosis

Shown is analysis of Httex1^{TC9}(97Q)-Cherry (or Cerulean) constructs transfected into AD293 cells. Where relevant, error bars indicate means ± SEM.

(A) Assessment of mechanism of cell death by a live-cell caspase-3 activation assay on cells earmarked as HBRi or PBRi 24 hr after transfection versus cells that die lacking inclusions. Differences were evaluated by two-tailed Fisher's exact test. QVD represents the broad-spectrum caspase inhibitor that blocks apoptosis.

(B) Survival curve of cells transfected with Httex1^{TC9}(97Q)-Cerulean measured from 24 hr after transfection. Differences were assessed by survival curve analysis and Mantel-Cox test.

(legend continued on next page)

the trigger of apoptosis from soluble Httex1 forms but does not disable the apoptotic machinery.

Inclusion Formation Correlates with Functional Quiescence

To determine why apoptosis is switched off as inclusions form, we examined the metabolic state of cells. Examination of the mitochondrial membrane potential using the MitoProbe reagent (Figure 3G) indicated cells with soluble Httex1(46Q) (ni) to be hyperpolarized and for cells with inclusions to be progressively hypopolarized relative to Httex1(25Q). Hyperpolarization of the mitochondrial membrane potential enhances off-pathway production of reactive oxygen species (Korshunov et al., 1997) and is consistent with soluble Httex1 triggering a state of stress concomitant with apoptosis. Indeed, cells with soluble Httex1(46Q) had an elevated CellRox signal, and those with inclusions were restored to the baseline level of the Httex1(25Q) counterpart (Figure 3H).

The hypopolarized membrane potential of cells with old inclusions suggested a state of quiescent metabolism. Hence, as a test for quiescence, we examined the ability of cells to translate a tetracycline-inducible reporter protein (Emerald). We found that the reporter could not be induced in cells that had pre-existing Httex1(97Q) inclusions, whereas cells with diffuse Httex1 showed no difference in induction compared with the control 25Q counterpart (Figure 3I). These data suggested that inclusion formation leads the cell into a state of broad functional quiescence.

Inclusions Appear to Originate from Httex1 Emerging from the Ribosome

Next we investigated the proteins that co-aggregated with HBRi- and PBRi-classified inclusions by quantitative proteomic analysis after sorting them by flow cytometry (as shown in Figure S2).

HBRi-enriched proteins included ribosome proteins and other ribonucleoproteins (Figure 4A; Table S2). PBRi-enriched proteins included other ribonucleoproteins, especially a subset of proteins that operate mRNA splicing or processing, a cluster of chaperones, and the Httex1 protein itself (Figure 4A; Table S2). The PBRi-enriched proteins also included proteins involved in RNA stress granule biology and neurodegenerative disease (Figure 4A). This included RNA-binding protein FUS and heterogeneous nuclear ribonucleoprotein (HNRNP) family proteins that, when mutated, cause amyotrophic lateral sclerosis (Kim et al., 2013; Vance et al., 2009). Classic components of stress granules, HSPB1 (HSP27) and PCBP1, were also enriched (Table S2; Kedersha et al., 1999). Many RNA granule proteins contain predicted prion-like domains that mediate liquid:liquid protein phase separation and/or "functional" amyloid scaffolding (Li et al., 2013). Hence, these proteins may be selectively recruited into the inclusion by a co-aggregation mechanism as Httex1 adopts an amyloid structure. Analysis of the prion domain propensity using the prion-like amino acid composition (PLAAC) algorithm (Lancaster et al., 2014) indicated that PBRi-enriched proteins were significantly more "prion-like" than a random set of proteins from the proteome (Figure 4B; Table S2). In contrast, HBRi-enriched proteins were not significantly more prion-like. A similar correlation was observed when the proteins were examined for glutamine content on the basis that polyQ-containing proteins are also able to recruit other polyQ proteins into the aggregates (Figure 4C). Of note was that several proteins enriched in the PBRi contained short stretches of glutamine-rich sequences (Table S2). To test whether prion-domain containing proteins can be recruited to the inclusions after the inclusion has initially formed, we co-expressed Httex1(97Q)-Cherry with TIA-1-GFP, a classic prion-like stress granule-associated protein that has a high PLAAC score of 22.2 and high glutamine content of 9.1% (Kedersha et al., 1999). Time-lapse images confirmed the recruitment of TIA-1 into Httex1 inclusions subsequent to Httex1 inclusion formation (Figure 4D).

DISCUSSION

Our study reconciles the large number of conflicting studies on the link between Httex1 inclusion formation and toxicity. In accord with the adaptive model of sequestration of toxic soluble Httex1 into inclusions, we showed that cells with soluble 97Q Httex1 have an elevated mitochondrial membrane potential, elevated levels of reactive oxygen species, and an elevated risk of triggering apoptosis. In accord with the model of pathogenic co-aggregation of essential cellular machinery, we showed that Httex1 inclusion formation progressively leads to a state of functional quiescence. Most importantly, our findings indicate that the prolonged survival of cells with inclusions can be explained by switching from a fast, directed death mechanism

(C) Mechanism of death on cells with respect to the length of time an inclusion has formed in cells measured by longitudinal imaging assays. Shown is mechanism of death, where apoptosis is indicated by a positive signal in the caspase-3 activation assay prior to cell lysis. The difference was evaluated by a two-tailed Student's t test.

(D) Fits of the data in (A)–(C) to the model shown. Relative rates are shown (k_n, rates of transition between states; $k_{Ap,n}$, rates of apoptosis where n represents the starting state).

(E) Fluorescence intensity of diffuse Httex1^{TC9}-Cerulean in cells at the time point of classification after ReAsH staining (24 hr after transfection). The differences were evaluated by two-tailed Student's t tests.

(F) Fluorescence intensity ratio of cytosolic:inclusion localized Httex1^{TC9}(97Q)-mCherry in cells with inclusions 1 hr prior to death. The differences were evaluated by two-tailed Student's t tests.

(G) Flow cytometry measurement of mitochondrial membrane potential with MitoProbe on AD293 cells 24 hr after transfection with Httex1^{TC9}-FT-fast (further gating details are shown in Figure S6).

(H) Equivalent experimental design to (G) using CellROX reagent for total cellular reactive oxygen species.

(I) Longitudinal induction of Emerald fluorescent protein expression (off a tetracycline regulatable promoter) in HeLa cells concurrently expressing Httex1^{TC9}(97Q)-Cerulean off a constitutive promoter. Time point indicates time after induction of Emerald expression by addition of tetracycline, which was 24 hr after transfection. Cells were categorized into those retaining diffuse Httex1 or inclusions upon addition of tetracycline.

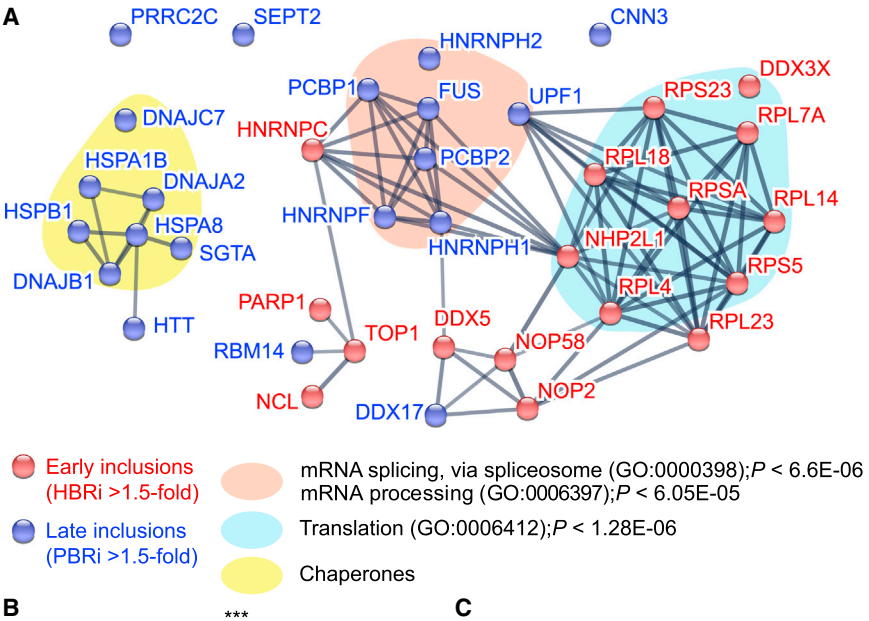

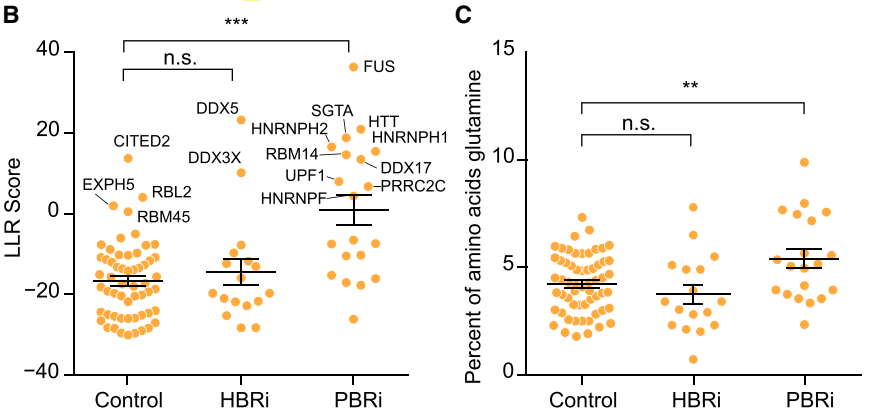

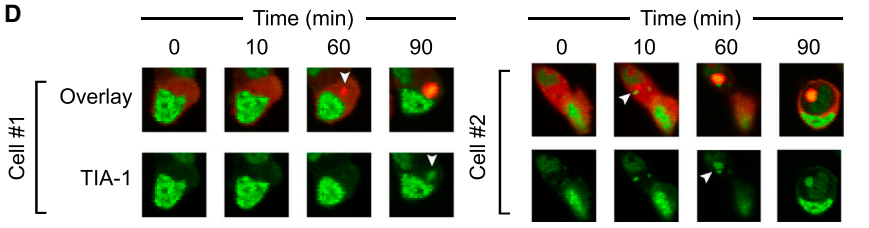

Figure 4. Early Inclusions Recruit Translational Machinery, whereas Mature Inclusions Attract Proteins with Predicted Prion-like Domains

(A) Protein-protein interaction network (STRING v10) of proteins identified in inclusions (the full list of proteins can be found in Table S2).

(B) Analysis of prion domains using the PLAAC algorithm. Higher log-likelihood ratios (LLR) relate to sequences in proteins more likely being a prion domain.

(C) Glutamine content versus control dataset of random human proteins (listed in Table S2).

(D) Recruitment of GFP-tagged prion domain protein TIA-1 (green) into Httex1(97Q)-Cherry inclusions (red) after the inclusion has formed. Two representative cells are shown in a time-lapse series.

(apoptosis) to a slow, passive one (necrosis) arising from cellular quiescence.

It remains to be established whether the disarmament of apoptosis is a by-product of quiescence or part of an active strategy to suppress toxicity. Clues can be gleaned from previous findings of expression of a 97Q form of Httex1 switching off apoptosis in sympathetic neurons (from rat superior cervical ganglia) and converting death to necrosis (King et al., 2008). However, in contrast to our findings, apoptosis could not be triggered with potent proapoptotic stimuli. Hence, it remains possible that quiescence is progressive; first by disabling the trigger for apoptosis and subsequently the machinery required to execute it.

Our data and proposed mechanism are summarized in Figure S7 (the legend of which includes an additional discussion). We postulate the presence of a quality control mechanism that clears aggregating proteins emerging from the ribosome in cells lacking inclusions. Prior data have shown that polyQ-expanded Httex1 is more efficiently degraded in cells lacking inclusions than the wild-type counterpart, which is consistent with an elevated clearance mechanism at this step (Ormsby et al., 2013; Tsvetkov et al., 2013). It follows that excessive blockage of this quality control mechanism could activate apoptosis, which provides a simple explanation for the proteotoxicity of the soluble Httex1. One candidate for this putative quality control mechanism is the ribosome quality control complex (RQC) (Brandman et al., 2012). The RQC is only beginning to be understood (in yeast) and functions to clear faulty mRNA sequences that lead to stalled ribosome-nascent protein complexes, such as non-sense-mediated decay or no-go decay (Brandman and Hegde, 2016; Lykke-Andersen and Bennett, 2014). UPF1 (RENT1), which plays a central role in non-sense-mediated decay (Lykke-Andersen and Bennett, 2014), was enriched in PBRis, suggesting a link to a mammalian RQC counterpart mechanism. However, we did not see any of the human counterparts of the yeast RQC in our data (Ltn1, Rqc1, Cdc48, or Tae2) (Brandman and Hegde, 2016; Lykke-Andersen and Bennett, 2014), suggesting that the RQC mechanism governing clearance of polyQ-expanded Httex1 in mammalian cells is different.

The cluster of heat shock protein family chaperones enriched with late-stage inclusions may point to a delayed attempt by the cell to degrade and clear the inclusions. Others have suggested

that stress granule formation aids in the management of proteome stresses by preventing apoptosis and reducing reactive oxygen species (Arimoto et al., 2008; Takahashi et al., 2013). Hence, it remains possible that inclusion formation involves an ancillary stress granule-associated proteostatic response that represses cellular metabolism. Of note, Huntingtin fragments in the soluble state can partition with stress granules, P bodies, and translational machinery (Culver et al., 2012; Savas et al., 2010).

In conclusion, our findings have important implications in pathology. It is conceivable that neurons may exist for extended periods of time in a quiescent state in vivo after they form inclusions. Such neurons would be expected to be viable but functionally suppressed and, hence, could impose large contributions to the state of neurological dysfunction in the disease process before the neurons die.

EXPERIMENTAL PROCEDURES

Expanded details of the methods are listed under Supplemental Experimental Procedures.

DNA Vectors and Constructs

The fluorescent proteins and human Httex1, Httex1^{TC9}, and Httex1^{TC1} as fusions to fluorescent proteins were expressed in vectors with cytomegalovirus (CMV) promoters. The gene encoding the fast fluorescent timer variant of mCherry was synthesized from the reported sequence (Subach et al., 2009). The GFP-TIA1 construct was kindly provided by Myriam Gorospe (NIA-NIH). The lentiviral vectors FUGW, psPAX2, and pCMV-VSV-G were used to generate lentiviral particles for expressing Httex1 variants.

Cell Culture

HEK293T, AD293, and HeLa cells (ATCC) were maintained in DMEM and Neuro2a in Optimem (Invitrogen). The medium was supplemented with 10% (v/v) fetal calf serum (FCS), 1 mM glutamine, and penicillin-streptomycin (pen-strep). The HeLa tet repressor line was generated with the T-REx system (Invitrogen). H9 human embryonic stem cells were induced into the neuronal lineage as described previously (Denham et al., 2012). The day 7 neurospheres were differentiated into cortical neurons using N2B27 medium supplemented with 1 μM N-[N-(3,5-Difluorophenacetyl)-L-alanyl]-S-phenylglycine t-butyl ester (DAPT) and 20 ng/mL brain derived neurotrophic factor (BDNF).

Western Blot

AD293 cells were transfected with pT-REx-Httex1(97Q)^{TC9}-Cerulean. After 24 hr, lysates (30 μg of cellular proteins) were subjected to western blot probed with anti-Huntingtin antibody (Abcam, ab109115).

Transfections and Transduction

Cell lines were transiently transfected with the vectors using Lipofectamine 2000 reagent (Life Technologies). Lentiviral particles were made using standard $CaCl_2$ transduction of HEK293T feeder cells and applied to day 7 cortical neurons. Inclusion formation was observed 5 days after lentiviral neuronal transduction.

Flow Cytometry

Cells were analyzed by PulSA with an LSRFortessa flow cytometer (BD Biosciences) as described previously (Ramdzan et al., 2012).

Confocal Imaging

Images of live or fixed cells were acquired with a Leica TCS SP5 microscope.

Slot Blot Assays

Neuro2a cells were lysed in 20 mM Tris, 2 mM $MgCl_2$, and 1% (w/v) Triton X-100 (pH 8.0) supplemented with cOmplete EDTA-free protease inhibitor cocktail pills (Roche) and 20 units/mL Benzonase (Novagen). The lysate was pelleted, and the insoluble fraction was resuspended in 200 μL Platereader buffer (20 mM Tris, 150 mM NaCl, 250 μM BAL, and 1 mM tris(2-carboxyethyl)phosphine [TCEP, pH 7.4]). ReAsH was added to 1 μM and incubated for 30 min. Samples were filtered through a nitrocellulose membrane and washed three times in Platereader buffer. The membranes were imaged on a fluorescent scanner (Typhoon, GE Healthcare).

FTIR Microscopy and Data Processing

Inclusions were purified as described for the proteomics experiments and then pelleted and washed in water. Recombinant Httex1-Cerulean fibrils were prepared as described previously (Olshina et al., 2010) and concentrated into pellets by centrifugation (12,000 × *g*, 15 min, 4°C). FTIR spectra were collected at the Infrared Microspectroscopy beamline at the Australian Synchrotron using a Bruker Hyperion 2000 IR microscope and Vertex 80v FTIR spectrometer.

ReAsH Staining, Stripping, and Restaining

For ReAsH staining, after 24 hr transfection (or transduction in the case of neurons), cells were washed twice with HBSS and stained with 1 μM ReAsH and 10 μM 1,2-ethanedithiol in Hank's balanced salt solution (HBSS) for 30 min at 37°C. The cells were then washed with 250 μM BAL for 15 min at 37°C, followed by a wash with HBSS.

For the stripping and restaining experiments, AD293 cells expressing pT-REx-Httex1^{TC9}(97Q)-Cerulean were labeled with ReAsH 24 hr after transfection as described above. The cells were imaged with a JuLI-stage microscope (NanoEnTek). ReAsH was stripped by 15-min treatment with 50 mM BAL in HBSS at 37°C followed by three washes with HBSS and then imaged again. Cells were then restained with ReAsH as described above at the time points indicated in the figures. Data were analyzed as described under Survival Analyses.

Survival Analyses

AD293 cells were co-transfected with pT-REx-HttEx1^{TC9}(97Q)-Cerulean (or pT-REx-HttEx1^{TC9}(97Q)-FT-Fast) and pT-REx-mCherry (or pT-Rex-Cerulean). 24 hr after transfection, the medium was refreshed. To block caspases, QVD-OPh (50 μM) was added at 24 hr. Cells were imaged longitudinally with a JuLI-stage fluorescence microscope (NanoEnTek). For analysis of cells assessing mechanism of death, apoptosis was measured using CellEvent caspase-3/7 green detection reagent (Life Technologies, catalog number C10423) according to the manufacturer's instructions.

AD293 cells were treated with MitoProbe $DiOC_2(3)$ (50 nM) or CellROX (5 μM) for 30 min in a cell culture incubator at 37°C, washed with PBS, and analyzed by flow cytometry as described previously (Ramdzan et al., 2012).

Sample Preparation for Proteomics

AD293 cells transfected with pT-REx-Httex1^{TC9}(97Q)-Cerulean were harvested 24 hr after transfection, lysed in 20 mM Tris, 2 mM $MgCl_2$, and 1% (w/v) Triton X-100 (pH 8.0) supplemented with cOmplete EDTA-free protease inhibitor cocktail pills (Roche) and 20 units/mL Benzonase (Novagen). The lysate was subjected to flow cytometry sorting on a BD FACS Aria III instrument to separate HBRis and PBRis. Sorted inclusions were washed in PBS three times, dissolved in formic acid for 30 min, and neutralized with 3 M Tris. Samples were digested with trypsin and differentially labeled by reductive dimethylation. Samples were matched for total protein levels.

NanoESI LC-MS/MS Analysis

Samples were analyzed by nano-electrospray ionization (nanoESI) liquid chromatography-tandem mass spectrometry (LC-MS/MS) and analyzed with nanoflow reverse-phase high-performance liquid chromatography (HPLC) and analyzed according to standard quantitative proteomic workflows (see details in the Supplemental Experimental Procedures).

Bioinformatics

PLAAC analysis was performed as described previously (Lancaster et al., 2014). Glutamine content was analyzed with the statistical analysis of protein sequences (SAPS) algorithm by European Molecular Biology Laboratory (EMBL) European Bioinformatics Institute (EBI) (http://www.ebi.ac.uk/Tools/seqstats/saps/).

Data Modeling

The data in Figures 3A–3C were modeled using a discrete state model in R, where the cells could exist in three states (1, diffuse; 2, early inclusion; 3, late inclusion) that could each have a distinct probability of undergoing apoptosis and dying.

HeLa tet Repressor Experiments

HeLa tet repressor cells were co-transfected with pGW-Httex1-mCherry and pT-REx-Emerald. 24 hr after transfection, the medium was refreshed and supplemented with 1 μg/mL tetracycline. The cells were imaged for 48 hr with a JuLI-stage live-cell imaging fluorescence microscope (NanoEnTek).

Statistics

The details of the tests are indicated in the figure legends. Non-significant (n.s.) results are defined in the figures for $p > 0.05$. p Values lower than 0.05 are coded as follows: *$p < 0.05$, **$p < 0.01$, ***$p < 0.001$, ****$p < 0.0001$.

ACCESSION NUMBERS

The accession number for the mass spectrometry data reported in this paper is ProteomeXchange Consortium: PXD005120.

SUPPLEMENTAL INFORMATION

Supplemental Information includes Supplemental Experimental Procedures, seven figures, and two tables and can be found with this article online at http://dx.doi.org/10.1016/j.celrep.2017.04.029.

AUTHOR CONTRIBUTIONS

Y.M.R., M.M.T., D.B.A., A.R.O., E.A.N., X.S., C.S.A., N.S.M., and S.W. designed and performed the experiments and analyzed the data. J.N., C.L.P., M.N.B., A.W.P., S.L.G., G.D., M.J.T., J.M.L.M., S.F., M.J.B., J.A.W., D.S., T.B., and G.E.R. designed experiments and/or analyzed data. Y.M.R. and D.M.H. conceived the work. D.M.H. directed the work and prepared the manuscript with contributions from all authors, and all authors contributed to discussions.

ACKNOWLEDGMENTS

This work was funded by a grant to D.M.H. from the Australian Research Council (FT120100039); grants/fellowships from the National Health and Medical Research Council Project to D.M.H. (APP1049458, APP1049459, and APP1102059), J.A.W. (APP1105801), A.W.P. (1044215), and D.B.A. (APP1072476); and a grant to D.M.H. from the Hereditary Disease Foundation. Part of this research was undertaken on the Infrared beamline at the Australian Synchrotron. This research was supported by the Victorian Life Sciences Computation Initiative, an initiative of the Victorian Government, Australia, at its Facility hosted at the University of Melbourne (UOM0017).

Received: October 26, 2016
Revised: March 16, 2017
Accepted: April 10, 2017
Published: May 2, 2017

REFERENCES

Arimoto, K., Fukuda, H., Imajoh-Ohmi, S., Saito, H., and Takekawa, M. (2008). Formation of stress granules inhibits apoptosis by suppressing stress-responsive MAPK pathways. Nat. Cell Biol. *10*, 1324–1332.

Arrasate, M., Mitra, S., Schweitzer, E.S., Segal, M.R., and Finkbeiner, S. (2004). Inclusion body formation reduces levels of mutant huntingtin and the risk of neuronal death. Nature *431*, 805–810.

Bodner, R.A., Outeiro, T.F., Altmann, S., Maxwell, M.M., Cho, S.H., Hyman, B.T., McLean, P.J., Young, A.B., Housman, D.E., and Kazantsev, A.G. (2006). Pharmacological promotion of inclusion formation: a therapeutic approach for Huntington's and Parkinson's diseases. Proc. Natl. Acad. Sci. USA *103*, 4246–4251.

Brandman, O., and Hegde, R.S. (2016). Ribosome-associated protein quality control. Nat. Struct. Mol. Biol. *23*, 7–15.

Brandman, O., Stewart-Ornstein, J., Wong, D., Larson, A., Williams, C.C., Li, G.W., Zhou, S., King, D., Shen, P.S., Weibezahn, J., et al. (2012). A ribosome-bound quality control complex triggers degradation of nascent peptides and signals translation stress. Cell *151*, 1042–1054.

Caserta, T.M., Smith, A.N., Gultice, A.D., Reedy, M.A., and Brown, T.L. (2003). Q-VD-OPh, a broad spectrum caspase inhibitor with potent antiapoptotic properties. Apoptosis *8*, 345–352.

Culver, B.P., Savas, J.N., Park, S.K., Choi, J.H., Zheng, S., Zeitlin, S.O., Yates, J.R., 3rd, and Tanese, N. (2012). Proteomic analysis of wild-type and mutant huntingtin-associated proteins in mouse brains identifies unique interactions and involvement in protein synthesis. J. Biol. Chem. *287*, 21599–21614.

Denham, M., Parish, C.L., Leaw, B., Wright, J., Reid, C.A., Petrou, S., Dottori, M., and Thompson, L.H. (2012). Neurons derived from human embryonic stem cells extend long-distance axonal projections through growth along host white matter tracts after intra-cerebral transplantation. Front. Cell. Neurosci. *6*, 11.

DiFiglia, M., Sapp, E., Chase, K.O., Davies, S.W., Bates, G.P., Vonsattel, J.P., and Aronin, N. (1997). Aggregation of huntingtin in neuronal intranuclear inclusions and dystrophic neurites in brain. Science *277*, 1990–1993.

Gidalevitz, T., Ben-Zvi, A., Ho, K.H., Brignull, H.R., and Morimoto, R.I. (2006). Progressive disruption of cellular protein folding in models of polyglutamine diseases. Science *311*, 1471–1474.

Kedersha, N.L., Gupta, M., Li, W., Miller, I., and Anderson, P. (1999). RNA-binding proteins TIA-1 and TIAR link the phosphorylation of eIF-2 alpha to the assembly of mammalian stress granules. J. Cell Biol. *147*, 1431–1442.

Kim, H.J., Kim, N.C., Wang, Y.-D., Scarborough, E.A., Moore, J., Diaz, Z., MacLea, K.S., Freibaum, B., Li, S., Molliex, A., et al. (2013). Mutations in prion-like domains in hnRNPA2B1 and hnRNPA1 cause multisystem proteinopathy and ALS. Nature *495*, 467–473.

King, M.A., Goemans, C.G., Hafiz, F., Prehn, J.H., Wyttenbach, A., and Tolkovsky, A.M. (2008). Cytoplasmic inclusions of Htt exon1 containing an expanded polyglutamine tract suppress execution of apoptosis in sympathetic neurons. J. Neurosci. *28*, 14401–14415.

Korshunov, S.S., Skulachev, V.P., and Starkov, A.A. (1997). High protonic potential actuates a mechanism of production of reactive oxygen species in mitochondria. FEBS Lett. *416*, 15–18.

Lajoie, P., and Snapp, E.L. (2010). Formation and toxicity of soluble polyglutamine oligomers in living cells. PLoS ONE *5*, e15245.

Lancaster, A.K., Nutter-Upham, A., Lindquist, S., and King, O.D. (2014). PLAAC: a web and command-line application to identify proteins with prion-like amino acid composition. Bioinformatics *30*, 2501–2502.

Leitman, J., Ulrich Hartl, F., and Lederkremer, G.Z. (2013). Soluble forms of polyQ-expanded huntingtin rather than large aggregates cause endoplasmic reticulum stress. Nat. Commun. *4*, 2753.

Li, Y.R., King, O.D., Shorter, J., and Gitler, A.D. (2013). Stress granules as crucibles of ALS pathogenesis. J. Cell Biol. *201*, 361–372.

Lykke-Andersen, J., and Bennett, E.J. (2014). Protecting the proteome: Eukaryotic cotranslational quality control pathways. J. Cell Biol. *204*, 467–476.

MacDonald, M.E., Ambrose, C.M., Duyao, M.P., Myers, R.H., Lin, C., Srinidhi, L., Barnes, G., Taylor, S.A., James, M., Groot, N., et al.; The Huntington's Disease Collaborative Research Group (1993). A novel gene containing a trinucleotide repeat that is expanded and unstable on Huntington's disease chromosomes. Cell *72*, 971–983.

Nucifora, L.G., Burke, K.A., Feng, X., Arbez, N., Zhu, S., Miller, J., Yang, G., Ratovitski, T., Delannoy, M., Muchowski, P.J., et al. (2012). Identification of novel potentially toxic oligomers formed in vitro from mammalian-derived expanded huntingtin exon-1 protein. J. Biol. Chem. *287*, 16017–16028.

Olshina, M.A., Angley, L.M., Ramdzan, Y.M., Tang, J., Bailey, M.F., Hill, A.F., and Hatters, D.M. (2010). Tracking mutant huntingtin aggregation kinetics in

cells reveals three major populations that include an invariant oligomer pool. J. Biol. Chem. *285*, 21807–21816.

Ormsby, A.R., Ramdzan, Y.M., Mok, Y.-F., Jovanoski, K.D., and Hatters, D.M. (2013). A platform to view huntingtin exon 1 aggregation flux in the cell reveals divergent influences from chaperones hsp40 and hsp70. J. Biol. Chem. *288*, 37192–37203.

Park, S.-H., Kukushkin, Y., Gupta, R., Chen, T., Konagai, A., Hipp, M.S., Hayer-Hartl, M., and Hartl, F.U. (2013). PolyQ proteins interfere with nuclear degradation of cytosolic proteins by sequestering the Sis1p chaperone. Cell *154*, 134–145.

Ramdzan, Y.M., Nisbet, R.M., Miller, J., Finkbeiner, S., Hill, A.F., and Hatters, D.M. (2010). Conformation sensors that distinguish monomeric proteins from oligomers in live cells. Chem. Biol. *17*, 371–379.

Ramdzan, Y.M., Polling, S., Chia, C.P., Ng, I.H., Ormsby, A.R., Croft, N.P., Purcell, A.W., Bogoyevitch, M.A., Ng, D.C., Gleeson, P.A., and Hatters, D.M. (2012). Tracking protein aggregation and mislocalization in cells with flow cytometry. Nat. Methods *9*, 467–470.

Savas, J.N., Ma, B., Deinhardt, K., Culver, B.P., Restituito, S., Wu, L., Belasco, J.G., Chao, M.V., and Tanese, N. (2010). A role for huntington disease protein in dendritic RNA granules. J. Biol. Chem. *285*, 13142–13153.

Schaffar, G., Breuer, P., Boteva, R., Behrends, C., Tzvetkov, N., Strippel, N., Sakahira, H., Siegers, K., Hayer-Hartl, M., and Hartl, F.U. (2004). Cellular toxicity of polyglutamine expansion proteins: mechanism of transcription factor deactivation. Mol. Cell *15*, 95–105.

Scherzinger, E., Lurz, R., Turmaine, M., Mangiarini, L., Hollenbach, B., Hasenbank, R., Bates, G.P., Davies, S.W., Lehrach, H., and Wanker, E.E. (1997). Huntingtin-encoded polyglutamine expansions form amyloid-like protein aggregates *in vitro* and *in vivo*. Cell *90*, 549–558.

Scherzinger, E., Sittler, A., Schweiger, K., Heiser, V., Lurz, R., Hasenbank, R., Bates, G.P., Lehrach, H., and Wanker, E.E. (1999). Self-assembly of polyglutamine-containing huntingtin fragments into amyloid-like fibrils: implications for Huntington's disease pathology. Proc. Natl. Acad. Sci. USA *96*, 4604–4609.

Subach, F.V., Subach, O.M., Gundorov, I.S., Morozova, K.S., Piatkevich, K.D., Cuervo, A.M., and Verkhusha, V.V. (2009). Monomeric fluorescent timers that change color from blue to red report on cellular trafficking. Nat. Chem. Biol. *5*, 118–126.

Takahashi, T., Kikuchi, S., Katada, S., Nagai, Y., Nishizawa, M., and Onodera, O. (2008). Soluble polyglutamine oligomers formed prior to inclusion body formation are cytotoxic. Hum. Mol. Genet. *17*, 345–356.

Takahashi, M., Higuchi, M., Matsuki, H., Yoshita, M., Ohsawa, T., Oie, M., and Fujii, M. (2013). Stress granules inhibit apoptosis by reducing reactive oxygen species production. Mol. Cell. Biol. *33*, 815–829.

Tsvetkov, A.S., Arrasate, M., Barmada, S., Ando, D.M., Sharma, P., Shaby, B.A., and Finkbeiner, S. (2013). Proteostasis of polyglutamine varies among neurons and predicts neurodegeneration. Nat. Chem. Biol. *9*, 586–592.

Vance, C., Rogelj, B., Hortobágyi, T., De Vos, K.J., Nishimura, A.L., Sreedharan, J., Hu, X., Smith, B., Ruddy, D., Wright, P., et al. (2009). Mutations in FUS, an RNA processing protein, cause familial amyotrophic lateral sclerosis type 6. Science *323*, 1208–1211.

Woerner, A.C., Frottin, F., Hornburg, D., Feng, L.R., Meissner, F., Patra, M., Tatzelt, J., Mann, M., Winklhofer, K.F., Hartl, F.U., and Hipp, M.S. (2016). Cytoplasmic protein aggregates interfere with nucleocytoplasmic transport of protein and RNA. Science *351*, 173–176.

Cell Reports, Volume *19*

Supplemental Information

Huntingtin Inclusions Trigger Cellular Quiescence, Deactivate Apoptosis, and Lead to Delayed Necrosis

Yasmin M. Ramdzan, Mikhail M. Trubetskov, Angelique R. Ormsby, Estella A. Newcombe, Xiaojing Sui, Mark J. Tobin, Marie N. Bongiovanni, Sally L. Gras, Grant Dewson, Jason M.L. Miller, Steven Finkbeiner, Nagaraj S. Moily, Jonathan Niclis, Clare L. Parish, Anthony W. Purcell, Michael J. Baker, Jacqueline A. Wilce, Saboora Waris, Diana Stojanovski, Till Böcking, Ching-Seng Ang, David B. Ascher, Gavin E. Reid, and Danny M. Hatters

SUPPLEMENTAL EXPERIMENTAL PROCEDURES

DNA vectors and constructs. pT-REx and pcDNA3.2 vectors expressing Emerald, as well as Httex1^{TC9} and Httex1^{TC1} with variable polyQ sequence lengths were prepared as described previously (Ramdzan et al., 2010; Ramdzan et al., 2012). For the tracer experiments that expressed mCherry, the mCherry cDNA was cloned into a pEGFP-C1 vector by swapping out the EGFP moiety. pGW1-based Httex1-mCherry constructs were prepared as described previously (Tsvetkov et al., 2010). The gene encoding the fast fluorescent timer variant of mCherry reported in (Subach et al., 2009) was synthesized and swapped, via restriction digestion and ligation based cloning strategies, for the Cerulean moiety in the pcDNA3.2 based vectors. The GFP-TIA-1 construct was kindly provided by Myriam Gorospe (NIA-NIH, Baltimore, USA).

The FUGW vector (Addgene Plasmid #14883), a gift from David Baltimore (Lois et al., 2002) was used for lentiviral generation of Httex1^{TC9} and Httex1^{TC1} constructs. The Httex1 constructs were inserted into the FUGW vector via the AgeI and EcoRI restriction sites. Packaging vectors psPAX2, a gift from Didier Trono (Addgene plasmid # 12260) and pCMV-VSV-G, a gift from Bob Weinberg (Addgene plasmid # 8454) (Stewart et al., 2003) were used to generate lentiviral particles.

Cell culture. AD293 and HeLa cells, obtained originally from the American Type Culture Collection (ATCC), were maintained in Dulbecco's modified Eagle medium (DMEM) (Life Technologies) supplemented with 10% (v/v) FCS, 1 mM glutamine, 100 U/mL penicillin (or 200 U/mL for AD293) and 100 µg/mL streptomycin (or 200 µg/mL for AD293) in a humidified incubator with 5% atmospheric CO_2 at 37 °C. Neuro2a cells, obtained originally from the ATCC, were maintained in Optimem medium (Life Technologies) supplemented with 10% FCS, 1 mM glutamine, 100 U/mL penicillin and 100 µg/mL streptomycin in a humidified incubator with 5% atmospheric CO_2. The HeLa tet repressor line was generated with the T-REx system (Invitrogen). From a pool of stable transformants, a high performance clonal line was selected using the tet-inducible pT-REx based Emerald fluorescent reporter protein. AD293 cells were plated on poly-L lysine coated plates and Neuro2a and HeLa cells on untreated tissue culture plates.

For the neuronal differentiation, H9 human embryonic stem cells were induced into the neuronal lineage with small molecules SB and LDN. Neuronal induction, neurosphere generation and expansion with EGF and FGF-2 were performed as described previously (Denham et al., 2012). The day 7 neurospheres were dissociated and differentiated into cortical neurons using N2B27 media supplemented with DAPT (γ-secretase inhibitor at 10 µM concentration) and BDNF 20 ng/mL. Neuronal lineage was confirmed by immunocytochemistry using antibodies β-III Tubulin, GFAP, and O4 in differentiated human cortical stem cells specific for neurons, astrocytes, and oligodendrocytes (R&D Systems, Catalog # SC024). The flow cytometry of the cell cultures further confirmed ~ 96-97% neuronal differentiation.

Western Blot. AD293 cells were transfected with pT-REx-Httex1^{TC9}-Cerulean (or were not transfected for the control baseline samples) and harvested 24 h post transfection by pelleting (200 *g*; 5 min; 24 ºC). Pellets were snap frozen in liquid nitrogen, thawed and resuspended in lysis buffer (20 mM Tris, 2 mM $MgCl_2$, 1% (w/v) Triton X-100, pH 8.0 supplemented with cOmplete, EDTA-free Protease Inhibitor Cocktail pills (Roche) and 20 Units/mL Benzonase (Novagen)). The lysates were matched for total protein by using the BCA kit (Thermo Scientific, # 23225). 30 µg (total protein) of lysates were subjected to SDS-PAGE using an 8.5% acrylamide resolving gel. The proteins were transferred to a PVDF membrane, and blocked with 5 % w/v skim milk powder in PBS and 0.1 % Triton X-100 for 1 hour at room temperature. The primary antibody was rabbit anti-Huntingtin (Abcam, ab109115) used at 1:5,000 dilution and applied for 1 h at room temperature in blocking solution. The secondary antibody was goat anti-rabbit HRP antibody (Invitrogen, cat # 656120) used at 1:10,000 dilution for 1 h at room temperature in blocking solution. HRP was detected using Enhanced Chemilumiscence protocol.

Transfections and transduction. AD293 and Neuro2a cells were transiently transfected with the vectors using Lipofectamine 2000 reagent (Life Technologies). Specific transfection conditions for the different culture vessel types at densities of 6×10^6 (T75 flasks), 5.5×10^4 (Ibidi 8-well µ-chamber), 2×10^5 (12-well plate) or 5×10^5 (6-well plate). The following day cells were transfected with 60, 1.25, 4 or 10 µL Lipofectamine 2000 and 24, 0.5, 1.6 or 4 µg vector DNA, respectively, as per the manufacturer's instructions (Life Technologies). The next day, the medium was changed, and the cells were subjected to ReAsH staining if required, according to the protocol as described previously (Ramdzan et al., 2012).

For the HeLa-Tet experiment, 2×10^5 cells were plated in a 12-well tissue culture plate. The following day the cells in each well were transfected with 4 µL Lipofectamine 2000 and 1.6 µg vector DNA.

For the neuronal transduction, the FUGW transfer plasmid containing Httex1^{TC1} and Httex1^{TC9} and packaging vectors were used to generate lentiviral supernatants using standard $CaCl_2$ transduction of HEK293T feeder cells. The supernatant after 48 hours post transduction was filtered and concentrated using PEG-*it* viral concentration solution (System Biosciences, Inc. USA). The Httex1^{TC9} and Httex1^{TC1} viral concentrates resuspended in neuronal differentiation media were added to the day-7 cortical neurons and aggregate formation was observed 5 days after lentiviral neuronal transduction.

Flow cytometry. For the analysis of cells expressing FlAsH-stained Httex^{TC9}-Cerulean, cells were analysed by PuLSA as previously described with an LSRFortessa flow cytometer (BD Biosciences) (Ramdzan et al., 2012). Fluorescent timer proteins were analysed using 561nm laser and 610/20 bandpass filter for the red form and 405nm laser 450/50 bandpass filter for the blue form. 'Old' and 'new' inclusions were gated using the ratio of the area of the red and blue forms. Pulse-shape gating analysis was done on the red form, using gating strategies described previously (Ramdzan et al., 2012).

Confocal Imaging. Images of live or fixed cells were imaging with a Leica TCS SP5 microscope. The objective used was HCX PL APO CS 63× oil immersion. Lasers used: 405 nm excitation, LP 425 nm emission – Hoescht/DAPI, ps-CFP; 458 nm excitation, LP 515 nm emission – CFP; 488 nm excitation, BP 525/50 nm emission – FlAsH; 561 nm excitation, LP 590 nm emission– mCherry. Single colour controls were used to establish and adjust to remove bleedthrough of the emission filter bandwidths.

Slot blot assays. 6×10^6 Neuro2a cells transfected with pT-Rex based Httex1-Cerulean constructs were harvested at the indicated timepoints in the figure by pelleting (200 *g*, 5 min, RT) and lysed in 20 mM Tris, 2 mM $MgCl_2$, 1% (w/v) Triton X-100, pH 8.0 supplemented with cOmplete, EDTA-free Protease Inhibitor Cocktail pills (Roche) and 20 Units/mL Benzonase (Novagen). The lysate was pelleted (12,000 *g*; 15 min; 4 °C), and the insoluble fraction was resuspended in 200 µL Platereader buffer (20 mM Tris, 150 mM NaCl, 250 µM BAL, 1 mM tris(2-carboxyethyl)phosphine, pH 7.4 (TCEP)). ReAsH was added to 1 µM and incubated for 30 min. The sample (200 µL) was filtered through a nitrocellulose membrane (0.2 µm pore size; pre-soaked with Platereader buffer) using a Bio-Rad Bio-Dot SF microfiltration unit, washed three times in Platereader buffer (100 µL per wash). The membranes were imaged on the fluorescent scanner (Typhoon, GE Healthcare) at an emission of 528 nm, laser 488 (Cerulean excitation) and at an emission of 670 nm, laser 633 (ReAsH excitation).

Fourier transformed InfraRed (FTIR) microscopy and data processing. Inclusions were purified as described for the proteomics experiments and then pelleted and washed in water. Recombinant Httex1-Cerulean fibrils were prepared as described previously (Olshina et al., 2010), and concentrated into pellets by centrifugation (12,000 *g*; 15 min; 4 ºC). FTIR spectra were collected at the Infrared Microspetroscopy beamline at the Australian Synchrotron (Clayton, VIC) using a Bruker Hyperion 2000 IR microscope and Vertex 80v FTIR spectrometer containing dual fluorescence (excitation filter: 420 – 490 nm; dichroic mirror 505 nm and emission filter: 520-1100 nm) and FTIR optics. Spectroscopy measurements were carried out using a microfabricated static liquid cell, as reported previously (Tobin et al., 2010). The inclusions, suspended in water, were sandwiched between two CaF_2 windows with one containing a patterned spacers (~8 µm thick) (MiniFAB Pty Ltd, Scoresby, Australia) and loaded into a ThermoFisher compression cell (Waltham, MA, USA). Individual inclusions were visualized using fluorescence mode on the microscope (fluorescein filter set) to identify and set clipping windows for a 5×5 µm^2 aperture. Bruker OPUS version 6.5 software was used for the acquisition of data method, and spectra were acquired in transmission mode with a spectral resolution of 4 cm^{-1} using Happ-Genzel apodization and two levels of zero filling. A total of 64 interferograms were co-added per spectrum. Background scans were obtained under identical conditions without inclusions for calculation of the sample absorbance spectrum. The use of hydrated samples for FTIR analysis minimises the effects of resonant Mie scattering on the shape of absorption peak profiles (Whelan et al., 2013), since scattering has been shown to result in experimental artefacts for dried biological samples measured in air (Bassan et al., 2009). The absence of a dip, or negative peak at around 1700 cm^{-1} on the high wavenumber edge of the amide I peak (Fig 2B and S3A) is evidence of a lack of scattering interference in the Amide I spectral profile. No correction was found to be necessary for the difference in total water content between the background position and each sample position. While variation in the broad water OH absorbance at around 1650 cm^{-1} between sample and background can result in variation in the total amide I peak intensity, the broad nature of this peak would be unlikely to alter the relative proportions of subcomponents of the amide I when comparing samples measured under similar conditions (Munro et al., 2010).

Spectra with maximum absorbance values between 0.1 and 1.0 in the amide I region were selected for analysis. Spectra were area normalised in the amide I region using OPUS software and second derivative spectra calculated

using the Savitsky-Golay algorithm with nine points of smoothing using the Unscrambler software version 10.1 (CAMO, Norway). Second derivative analysis also largely removes the broader spectral contribution arising from variation between sample and background in the OH absorbance peak of water.

Principal component analysis (PCA) (Unscrambler software version 10.1) with full cross validation was used to examine the general trends in the dataset (1720 – 1600 cm^{-1}). PCA scores plots were used to visualise any clustering of the samples, and PC1 loadings data were used to determine the spectral region that most contributed to the variance in the dataset (Heraud et al., 2010; Tobin et al., 2010).

ReAsH staining, stripping and restaining. For ReAsH staining, after 24 h transfection (or transduction in the case of the neurons) cells were washed twice with HBSS and stained with 1 μM ReAsH and 10 μM 1,2-ethanedithiol in HBSS for 30 min at 37 °C. The cells were then washed with 250 μM BAL for 15 min 37 °C, followed by a wash with HBSS.

For the stripping and restaining experiments, HEK293 cells expressing pT-REx-Httex1^{TC9}(97Q)-Cerulean were labelled with ReAsH at 24 hours post transfection as described above. The cells were imaged under the JuLI-stage microscope. ReAsH was stripped by a 15 min treatment with 50 mM BAL in HBSS at 37 °C, followed by 3 washes with HBSS, and then and imaged again. We validated that this treatment did not lead to altered toxicity by survival curve analysis. Cells were then restained with ReAsH as described above at the time points indicated in the figures. Data was analysed as described above under "Survival analyses".

Survival analyses. For survival analysis of cells with versus without inclusions, AD293 cells in 12-well plate format were co-transfected with pT-REx-HttEx1^{TC9}(97Q)-Cerulean and pT-REx-mCherry, as an independent tracer of cell integrity as described previously (Arrasate et al., 2004). In addition, pT-Rex-mCherry was used as a proxy for Httex1 levels in the cell on the basis that it would correlate with the efficiency of transfection for different cells. 24 hours after transfection, the media was refreshed. For the QVD treatment, QVD was added to the media to a final concentration of 50 μM, 24 h after transfection. Cells were then imaged longitudinally with the JuLI-stage fluorescence microscope at 15 min intervals for 130 h. Channels used: GFP for Cerulean (Excitation: 466/40, Emission: 525/50), RFP for mCherry (Excitation: 525/50, Emission: 580 LP). Death was recorded as the time points at which mCherry fluorescence was lost. Cells that drifted from focus were censored. Mean mCherry intensity was recorded in a region of interest encapsulating the cytosol of each cell and used as a proxy for Httex1 expression level. Image processing was performed with the FIJI version of ImageJ (Abramoff et al., 2004). Survival curve analysis was performed in Prism software (GraphPad).

For analysis of cells comparing the HBRi and PBRi categories, the protocol was as above with the following differences. AD293 cells were co-transfected with pT-REx-Httex1^{TC9}-mCerulean and pT-REx Cerulean as a tracer for cellular integrity. Since we were focused on inclusions only in these experiments, we posited that the Cerulean tracer would be largely sterically excluded from Httex1-Cerulean inclusions meaning the Cerulean signal in inclusions should be a good indicator of Httex1 levels in the inclusion. In addition, because Httex1 aggregation into inclusions is highly cooperative leaving only trace remnants of cytosolic Httex1 (Hipp et al., 2012), we posited that most of the cytosolic Cerulean signal should arise from the tracer construct (although we note that this is an imprecise approximation – as evidenced by the levels of soluble Httex1 in Fig 3E). Hence we used cytosolic Cerulean fluorescence as our proxy for expression level of Httex1-Cerulean in the cell. This approach to use the same fluorescence color tracer as the Httex1 construct was necessitated by the limited channels of the JuLI-stage microscope when we include the ReAsH channel. 24 hours after transfection, the cells were washed twice with HBSS media and labeled with 1 μM ReAsH in Hank's buffered salt solution (HBSS) containing 10 μM 1,2-ethanedithiol. For the QVD experiments, QVD was added at this point as described above. Cells were then imaged with the JuLI-stage microscope; Cerulean was tracked in GFP channel, ReAsH was tracked in RFP channel. For analysis, cells were assessed for inclusion formation immediately after ReAsH staining and categorized into the HBRi and PBRi categories. This was achieved by assigning a region of interest (ROI) (3 × 3 pixels) on top of the inclusion and using the mean Cerulean and ReAsH fluorescence ratios to classify HBRi and PBRi. The HBRi category was defined as having a ratio 10% above the minimum ReAsH/Cerulean ratio of a positive control (TC1 variant of Httex1, which binds ReAsH unhindered in the aggregated state (Ramdzan et al., 2010)). The PBRi category was defined as having the ratio 10% below the minimum of the TC1 control ReAsH/Cerulean ratio. Cerulean fluorescence in the cytosol of the cells with inclusions were recorded as a proxy for expression level. Death was assayed by loss of cytosolic Cerulean fluorescence.

For analysis of cells assessing mechanism of death, the protocol was as above using AD293 cells co-transfected with pT-REx-Httex1^{TC9}-mCherry (25Q or 97Q variants) and pT-REx mCherry as a tracer. 24 hours after transfection,

media was refreshed and supplemented with 5 μM CellEvent Caspase-3/7 Green Detection Reagent (Life Technologies, cat # C10423). For the analysis, Caspase activation was tracked in the GFP channel with an apoptotic event marked as when the signal in the cytosol exceeds two fold greater than background fluorescence (of Caspase non-reactive cells). mCherry was tracked in the RFP channel.

For the treatments with apoptotic stimulants, AD293 cells in 12-well plate format were transfected with pT-REx-HttEx1TC9(97Q)-FT-Fast. 24 hours after transfection, the media was refreshed and contained 5 μM CellEvent Caspase-3/7 Green Detection Reagent and 1 μM of staurosporine, 10 μM of etoposide or 10 μM of ABT-737, respectively. Staurosporine is a broad spectrum but potent inhibitor of protein kinases that activates apoptosis through mechanisms that are not well understood (Belmokhtar et al., 2001). Etopiside is an inhibitor of topoisomerase II and impairs DNA replication, leading to activation of apoptosis (Hande, 1998). ABT-737 specifically targets the core apoptotic machinery by inhibiting pro-survival proteins Bcl-2, Bcl-xL, and Bcl-w (van Delft et al., 2006). The mechanism of death was assessed as described above.

Mitoprobe and CellRox. For the MitoProbe experiments, AD293 cells in 12-well plate format were detached in 1 mL of PBS by pipetting and left as suspensions in the plate. MitoProbe $DiOC_2(3)$ (Life Technologies cat # M34150) was added to a final concentration of 50 nM and the cells were incubated for 30 minutes in a humidified incubator at 37 °C and 5% atmospheric CO_2. After addition of 2 mL PBS, the cells were pelleted (120 *g*; 6 minutes; room temperature) and resuspended in 500 μL PBS for immediate analysis by flow cytometry as described previously (Ramdzan et al., 2012).

For CellROX experiments, CellROX (Life Technologies cat #C10422) was added to plated AD293 cells to a final concentration of 5 μM and the cells were incubated for 30 minutes in a humidified incubator at 37 °C and 5% atmospheric CO_2. Media was removed and cells were washed 3 times with 1 mL pre-warmed PBS. Cells were detached in 750 μL of PBS by pipetting for immediate analysis by flow cytometry.

Sample preparation for proteomics. AD293 cells transfected with pT-REx-Httex1^{TC9}-Cerulean in 3 replicates were harvested at 24 h post transfection by pelleting (200 *g*; 5 min; 24 ºC), snap-freezing, thawing and resuspension in lysis buffer (20 mM Tris, 2 mM $MgCl_2$, 1% (w/v) Triton X-100, pH 8.0 supplemented with cOmplete, EDTA-free Protease Inhibitor Cocktail pills (Roche) and 20 Units/mL Benzonase (Novagen)). The lysate was subjected to flow cytometry sorting on a BD FACS Aria III instrument, and HBRi and PBRi inclusions were sorted as described in Fig S2 and treated as paired replicates. Sorted inclusions were pelleted (3,000 *g*; 5 min; 24 ºC), resuspended in PBS and washed 3 times by pelleting as above and resuspension in PBS. The final pellets were harvested by pelleting (12,000 *g*, 5 min, 24 ºC) and dissolved in 10 μL neat formic acid for 30 min at 37 ºC in a shaking microfuge tube incubator (250 rpm). The solution was neutralized to pH 7.0 by titration with 3 M Tris. The protein concentration in the sample was determined by a Bradford assay using BSA as mass standard. 200 μg of total protein was mixed with 100 μL of 8 M Urea, 50 mM triethylammonium bicarbonate (TEAB), 10 mM tris(2-carboxyethyl)phosphine, pH 8.0 and then prepared for proteomics using a Filter Aided Sample Preparation (FASP) Protein Digestion Kit (Expedeon). Proteins were digested with 1 μg trypsin at 24 ºC overnight. Resultant peptides were cleaned with a solid-phase extraction procedure (SPE) by acidifying the solution in 1% (v/v) formic acid; pre-washing the cartridge (Oasis HLB 1 cc Vac Cartridge, product number 186000383, Waters Corp., USA) with 1 mL of 80% acetonitrile (ACN) containing 0.1% trifluoroacetic acid (TFA) and washing it with 1.2 mL of 0.1% TFA 2 times by applying vacuum manifold; loading the sample on the cartridge and washing the sample with 1.5 mL of 0.1% TFA; eluting the sample with 0.8 mL of 80% ACN containing 0.1% TFA and collecting in 1.5 mL Eppendorf tubes; speedvac drying for 20 min to reduce concentration of ACN and lyophilization by freeze drying (Virtis, SP Scientific). Freeze dried peptides were resuspended in 100 μL of 100 mM of triethylammonium bicarbonate (TEAB) followed by differential labelling by reductive dimethyl labelling using 4 μL of 4% (vol/vol) formaldehyde $–CH_2O$ (light label), CD_2O (medium label) (HBRi – medium, PBRi – light) and 4 μL of 0.6 M sodium cyanoborohydride. The reaction was quenched by addition of 16 μL of 1% ammonium hydroxide followed by 8 μL of neat formic acid. Samples were matched, 1:1 w/w for total protein levels, calculated using the bicinchoninic acid assay with bovine serum albumin as mass standard.

NanoESI-LC-MS/MS analysis. Samples were analysed by nanoESI-LC-MS/MS using an LTQ Orbitrap Elite mass spectrometer (Thermo Scientific) fitted with nanoflow reversed-phase-HPLC (Ultimate 3000 RSLC, Dionex). The nano-LC system was equipped with an Acclaim Pepmap nano-trap column (Dionex – C18, 100 Å, 75 μm × 2 cm) and an Acclaim Pepmap RSLC analytical column (Dionex – C18, 100 Å, 75 μm × 15 cm). Typically for each LC-MS/MS experiment, 2 μL of the peptide mix was loaded onto the enrichment (trap) column at an isocratic flow of 5 μL/min of 3% CH_3CN containing 0.1% formic acid for 5 min before the enrichment column is switched in-line with

the analytical column. The eluents used for the LC were 0.1% v/v formic acid (solvent A) and 100% CH_3CN/0.1% formic acid v/v (solvent B). The gradient used was 3% B to 25% B for 20 min, 25% B to 40% B in 2 min, 40% B to 80% B in 2 min and maintained at 80% B for the final 2 min before equilibration for 6 min at 3% B prior to the next analysis. All spectra were acquired in positive mode with full scan MS spectra scanning from m/z 300–2000 in the FT mode at 240,000 resolution after accumulating to a target value of $1.00e^6$ with maximum accumulation of 200 ms. Lockmass of 445.120024 was used. The 20 most intense peptide ions with charge states ≥2 were isolated at a target value of 5,000 and fragmented by low energy CID with normalized collision energy of 30 and activation Q of 0.25. Dynamic exclusion was activated for 45 s.

Data analysis was carried out using Proteome Discoverer (version 2.1.0.81; Thermo Scientific) with the Mascot search engine (Matrix Science version 2.4.1). Data was filtered against the Swissprot *Homo sapiens* database (version 2015_07: Jun-24, 2015; 548872 entries). The search was conducted with 20 ppm MS tolerance, 0.6 Da MS/MS tolerance, 2 missed cleavages allowed. The following modifications were allowed: Oxidation (M), Acetyl (Protein N-term), Dimethyl (K), Dimethyl(N-Term) (N-term), Dimethyl:2H(4) (K), Dimethyl:2H(4) (N-term) (Variable); Carbamidomethyl (C) (Fixed).

Light and medium dimethyl labelled peptide pairs were established with a 2 ppm mass precision, a signal to noise threshold of 1, and filtered for a minimum Mascot ion score of 30. The retention time tolerance of isotope pattern multiplets was set to 0.8 min. 2 single peak/missing channels were allowed for peptide identification. The false discovery rate (FDR) maximum setting for peptide identification and peptide spectrum matches was set at 5 % (actual FDR used was 0.5% for all identified peptides). Protein identifications were determined using an FDR of 1%. Proteins were filtered for those that had at least two unique peptides in at least two replicates. The common contaminant, Keratin, was excluded from the final dataset. Protein groups for peptide uniqueness was not considered.

The peptide and protein quantifier node from Proteome Discoverer was used for quantification. Quant values with 0 missing channels were used and only unique peptides were used for quantification. Otherwise all default parameters were used in the software. In essence, the protein abundance in each replicate was calculated by summation of the unique peptide abundances that were used for quantitation (light and medium dimethyl derivatives). In the cases where quan values were missing or were apparent outliers to the other two replicates, raw data was manually checked and added or adjusted where relevant (these abundance values are highlighted in italic in Table S2 – under *Expanded Proteomics data*). The protein ratios (light versus medium labels) were manually calculated from the protein abundances as described previously (Kim et al., 2011). Data were normalized by standardizing the protein ratios to the median of each replicate. These correction values were multipliers of (replicate 1: 1.0989), (replicate 2: 1.4492) and (replicate 3: 1.8182).

Bioinformatics. PLAAC analysis was performed online (plaac.wi.mit.edu/) (Lancaster et al., 2014) with the following parameters: (minimal length for prion domain = 60; organism specific background from *H. sapiens;* continuous interpolation between organism-specific frequencies selected by α=0. A control set of 60 random proteins (Table S1) was generated from a list of the human proteome (Uniprot UP000005640; July 9 2016).

For protein-protein network analysis, STRING (version 10.0) was used (Szklarczyk et al., 2015) using active interaction sources parameters on for Experiments, Databases, Co-expression neighborhood, Gene Fusion and Co-occurrence. The minimimum required interaction score setting was 0.7 (high confidence).

For gene ontology analysis, data was analyzed by the PANTHER Overrepresentation Test (PANTHER version 11.0, 2016-07-15) using the PANTHER GO-Slim Biological Process dataset. Results were filtered for $P<0.05$.

Data modeling. The dynamics of the experimentally observed data in Fig 3A and 3C were modelled using a discrete state model in R, where the cells could exist in 3 states (1: diffuse, 2: early inclusion or 3: late inclusion) that could each have a distinct probability of undergoing apoptosis and dying. The rates were modelled using a simple one state exponential functions, yielding the rates of transition between states (k_n), rates of apoptosis ($k_{App,n}$) and initial time before transition ($X_{0,n,}$) where n refers to the starting state. The model was fitted using 10-fold cross validation, with the final correlation to the experimental data of 0.96. The relative risk of each population to undergo apoptosis was calculated using the Mantel-Cox method. The Asymmetrical profile likelihood confidence intervals were calculated as described previously (Venzon and Moolgavkar, 1988).

HeLa tet-repressor experiments. HeLa-tet repressor cells in 12-well plate format were co-transfected with equivalent plasmid masses of pGW-Httex1-mCherry and pT-REx-Emerald. 24 hours after transfection, the media

was refreshed and supplemented with 1 μg/mL tetracycline. The cells were imaged for 48 hours recording images at 15 min intervals with a JuLI Stage live cell imaging fluorescence microscope (NanoEnTek, Korea), collecting GFP and RFP fluorescence channels. For data analysis, cells were tracked for Httex1 expression and inclusion status via Cherry fluorescence. Cells were manually categorized into inclusion or non-inclusion status and median cellular Emerald fluorescence was tracked over time within a region of interest drawn to encompass the cytosol.

Statistics. The statistical tests were performed in Prism software (GraphPad). Details of tests are indicated in the figure legends. Non-significant results (n.s.) were defined on the figures for $P > 0.05$. P values lower than 0.05 are coded as *, $P<0.05$; **, $P<0.01$; ***, $P<0.001$; ****, $P < 0.0001$. For multiple tests on the same figure, the different tests are distinguished with * and # symbols.

Table S1: Full list of parameters from fit to model. Relates to Fig 3D.

Parameter*	Unit	Value	95% confidence interval
k_1	h^{-1}	0.02	
k_2	h^{-1}	0.07	
$k_{app,1}$	h^{-1}	0.037	0.035-0.042
$k_{app,2}$	h^{-1}	0.017	0.011-0.023
$k_{app,3}$	h^{-1}	0.007	0.005-0.017
$X_{0,1}$	h	31	
$X_{0,2}$	h	53	
$X_{0,3}$	h	44	

***$X_{0,n}$** denotes start time for transition to apoptosis, where n refers to state (1, Diffuse; 2, early inclusion; 3, late inclusion). Other parameters are defined in Fig 3D.

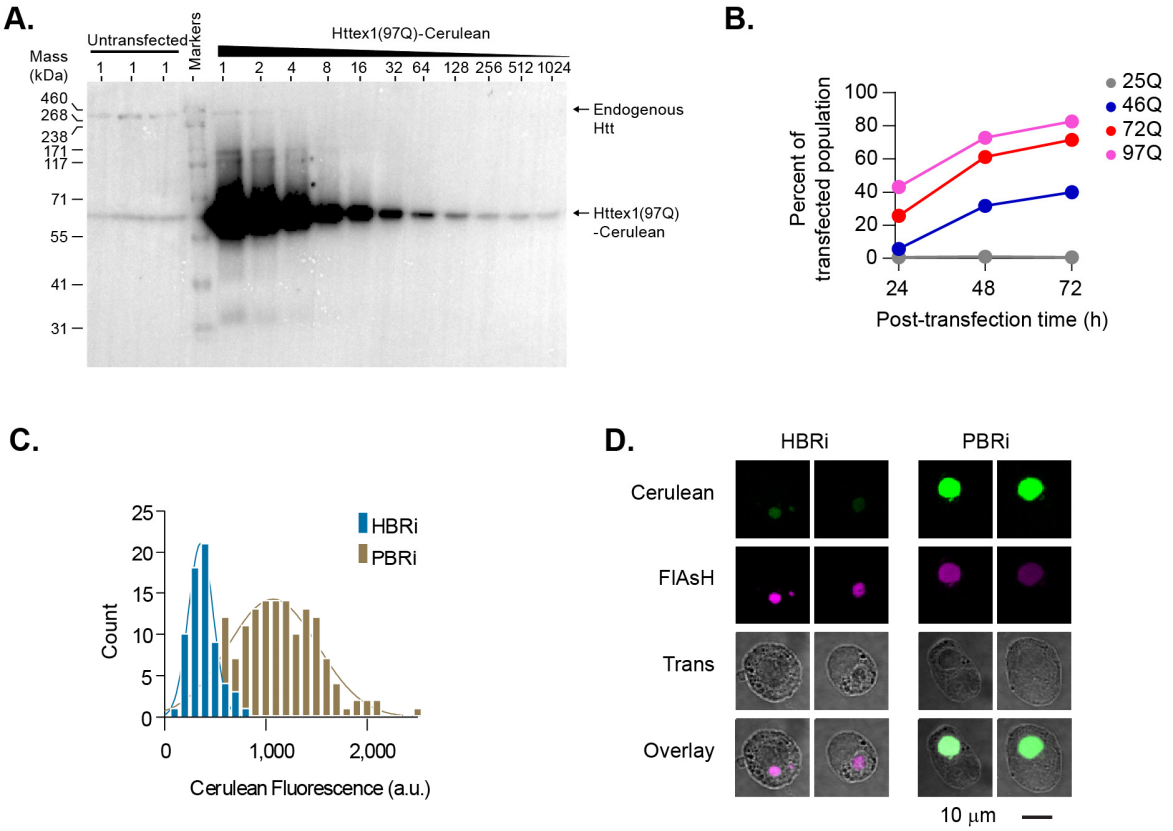

Figure S1: Expression levels of Httex1 and extent of aggregation of Httex1 into HBRi and PBRi categories in the AD293 cell model (Relates to Fig 1). **A.** Western Blot to show relative expression level of Httex1 to endogenous Htt. 30 μg of cell lysate was loaded and serial dilutions thereof (dilution factors shown above lanes). Lanes on left represent untransfected AD293 cells. Lanes on right indicate serial dilution of AD293 cells transfected with Httex1^{TC9}(97Q)-Cerulean. The Blot was probed with anti-Huntingtin (Abcam, ab109115). Arrows indicate the anticipated masses for full length endogenous Htt and the transfected construct. **B**. Formation of HBRi class of inclusions in AD293 cells transfected with Httex1^{TC9}-Cerulean of indicated polyQ lengths, measured by flow cytometry (relates to Fig 1C). **C**. HBRi and PBRi category dependence on expression level in AD293 cells measured 24 h after post transfection. **D.** Visual inspection of inclusions in HBRi and PBRi classified Neuro2a cells expressing Httex1^{TC9}(97Q) 24 h post transfection.

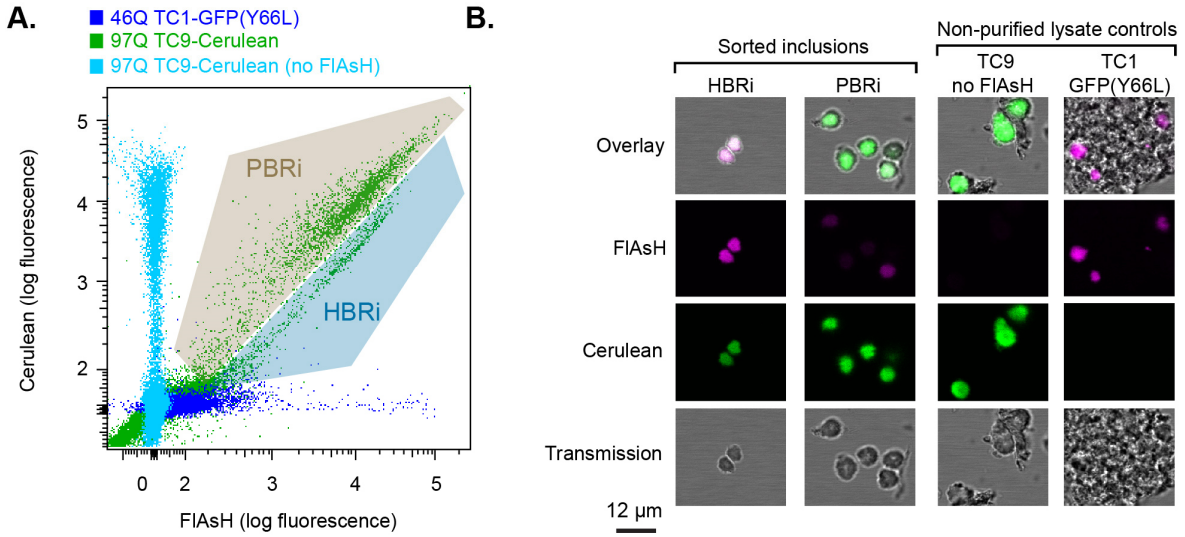

Figure S2: Visualization and recovery of HBRi and PBRi inclusions. Relates to Fig 2 and 5. **A.** Cell lysate was prepared under non-denaturing conditions and applied directly to flow cytometry. Cells expressing the indicated constructs were labelled with FlAsH prior to lysis. The TC1 acts as a positive control. It denotes an alternative biosensor form of Httex1 containing a tetracysteine tag insertion at a different sequence position: this variant shows similar biarsenical reactivity whether Httex1 is in monomeric or amyloid state (Ramdzan et al., 2010). The GFP Y66L mutations renders loss of fluorescence, but retains foldedness of the GFP. **B**. Confocal micrographs of inclusions purified by flow cytometry of populations indicated in panel A.

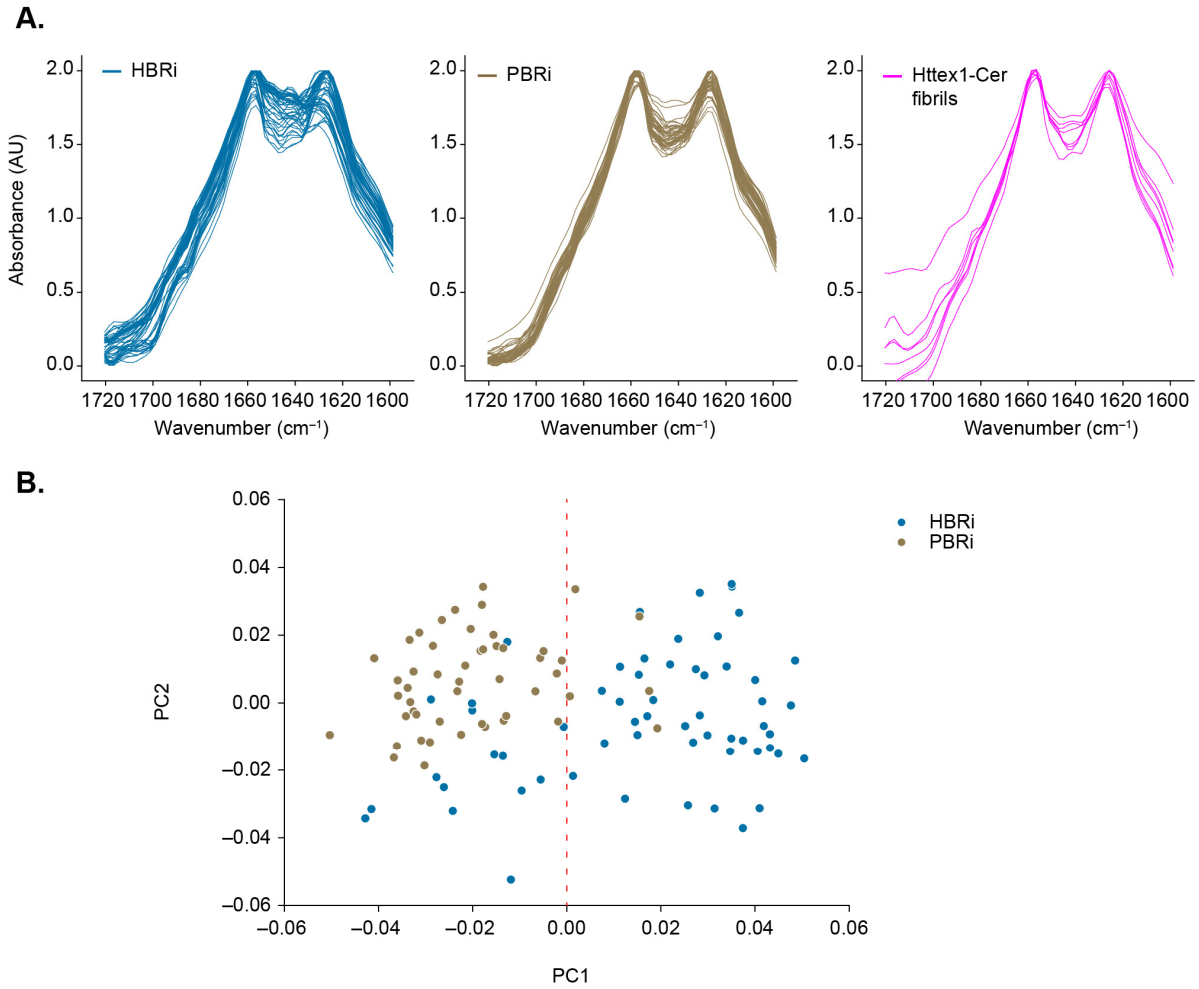

Figure S3: Variation in the HBRi and PBRi FTIR spectra. **A**. Individual FTIR spectra of inclusions or protein aggregates. These data correspond to the average spectra shown in Fig 2B. **B.** Principle component analysis of the Infrared (IR) spectra (Heraud et al., 2010). The PCA scores plot was used to illustrate clustering of the HBRi or PBRi inclusions where each point represents an IR spectrum from a single inclusion. As a general trend, PBRi or HBRi aggregates clustered on the left or right, respectively, of the first principal component (PC1; x-axis; i.e. the absoption region that accounts for the largest proportion of the variation in the data), demonstrating that PBRi and HBRi aggregates have distinct secondary structures. A proportion of the HBRi points, however, appear on the left, indicating that a sub-population of the HBRi aggregates are similar to PBRi aggregates in their protein secondary structure. PC1 loadings data was used to determine the spectral region that contributes most most significantly to the differences observed in the protein secondary structure of PBRi and HBRi aggregates. The corresponding loadings plot (data not shown) indicates that the protein β-sheet structure and α-helical structure (loadings at ~1658 cm^{-1} and ~1626 cm^{-1}, respectively) are the key discriminators in the structral differences observed for the inclusions. These wavenumbers are important since they can be used to differentiate aggregate maturity (i.e. those aggregates with higher loadings at ~1626 cm^{-1} have more β-sheet and are more amyloid-like).

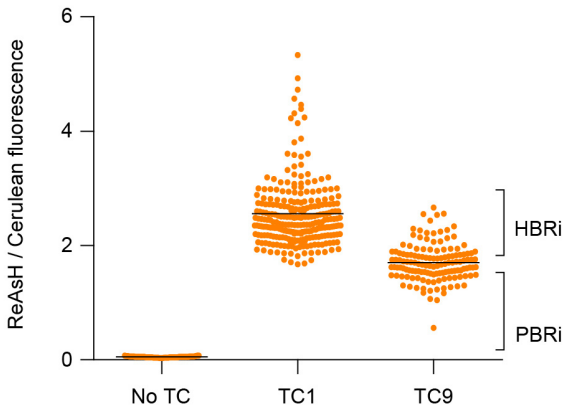

Figure S4: Strategy to classify HBRi and PBRi categories from microscopy data. Relates to Fig 3. Cells expressing Httex1(97Q)-Cerulean either lacking a TC tag, containing the TC9 tag or another tag, TC1, that labels biarsenical dyes efficiently in the aggregated state (Ramdzan et al., 2010) are used to calibrate ReAsH reactivity. The HBRi and PBRi cells are assigned by ratio of ReAsH/Cerulean fluorescence as indicated on cells labelled with ReAsH 24 h after transfection. Data shows mean fluorescence measurements of individual inclusions; bars show population means.

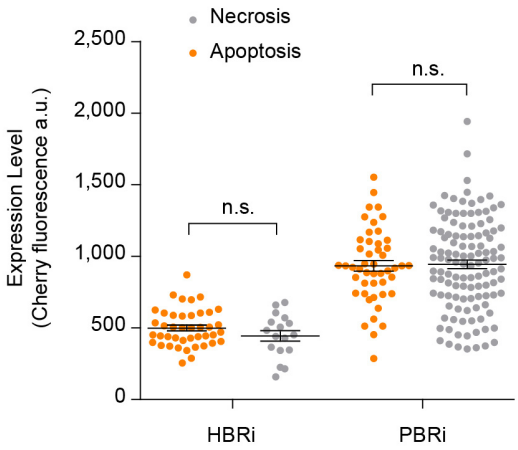

Figure S5: Mechanism of cell death of cells with inclusions is not dependent on expression level. Relates to Fig 3. Data shows mean cytoplasmic fluorescence of mCherry co-transfected with Httex1-Cerulean Y66L as a tracer for gene dose. The mCherry levels were assessed at 24 h transfection after staining the cells with ReAsH to classify the HBRi and PBRi inclusions. Data shows individual cells, with population mean and SEM. Differences were assessed with a two-tailed Student's t-test.

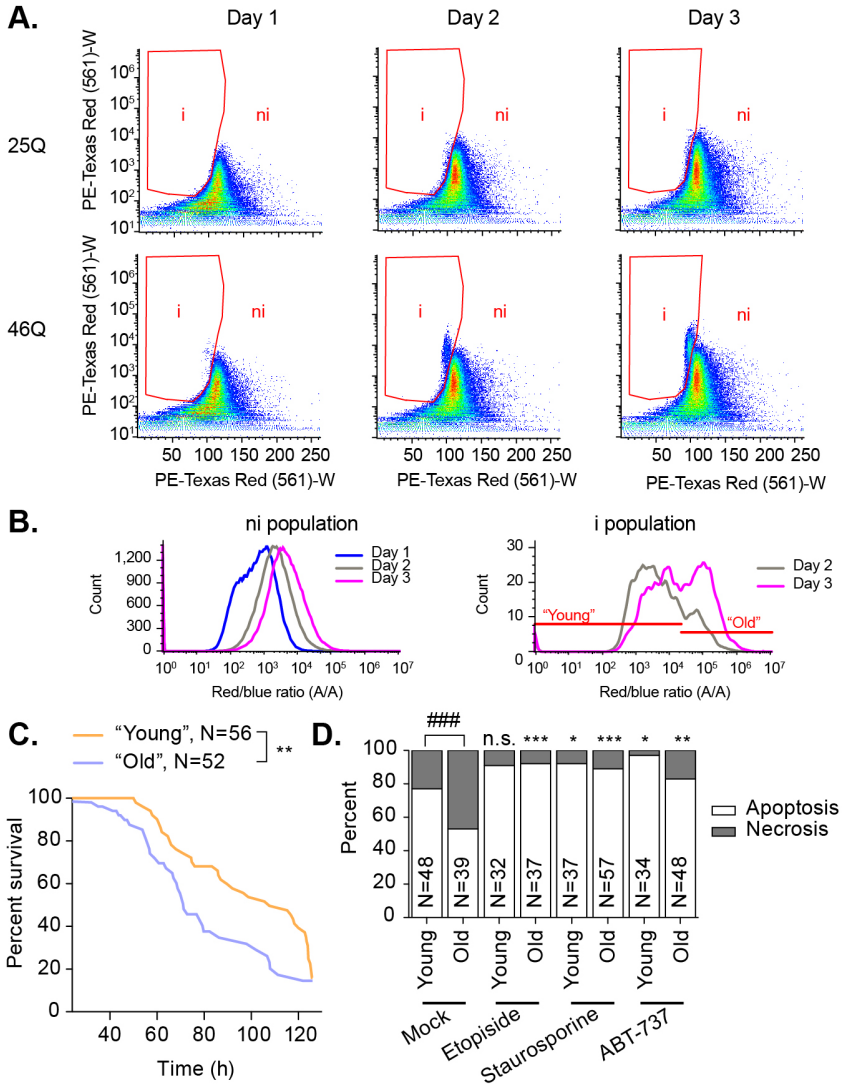

Figure S6: Use of fluorescent timer protein to track inclusion age by flow cytometry and impact of apoptotic stimulants. Relates to Fig 3. AD293 cells were used**. A.** Gating strategy to track inclusions and non-inclusions for Httex1-FT-Fast fusions by pulse shape analysis on the red fluorescence channel (PE-Texas Red). Since fluorescence properties change over time, gates for i and ni were adjusted manually for each time point post transfection. **B.** Histogram of red/blue fluorescence in the ni and i gates. This ratio was calculated from the PE-Texas Red-A and DAPI-A channels. **C.** Survival curve of cells transfected with Httex1(97Q)-FT-Fast. Cells with Young and Old inclusions were classified at 24 post transfection and tracked for survival thereon. Mantel-Cox test results indicated. **D.** Proportion of cells that died by apoptosis or necrosis expressing Httex1(97Q)-FT-Fast. Cells were classified as apoptotic if they showed fluorescence from the caspase 3 activation assay prior to cell lysis. Shown are 2-tailed Fisher's Exact test results between treatment and mock (* (and the n.s.), Young vs Young and Old vs Old comparisons; #, Young vs Old comparison).

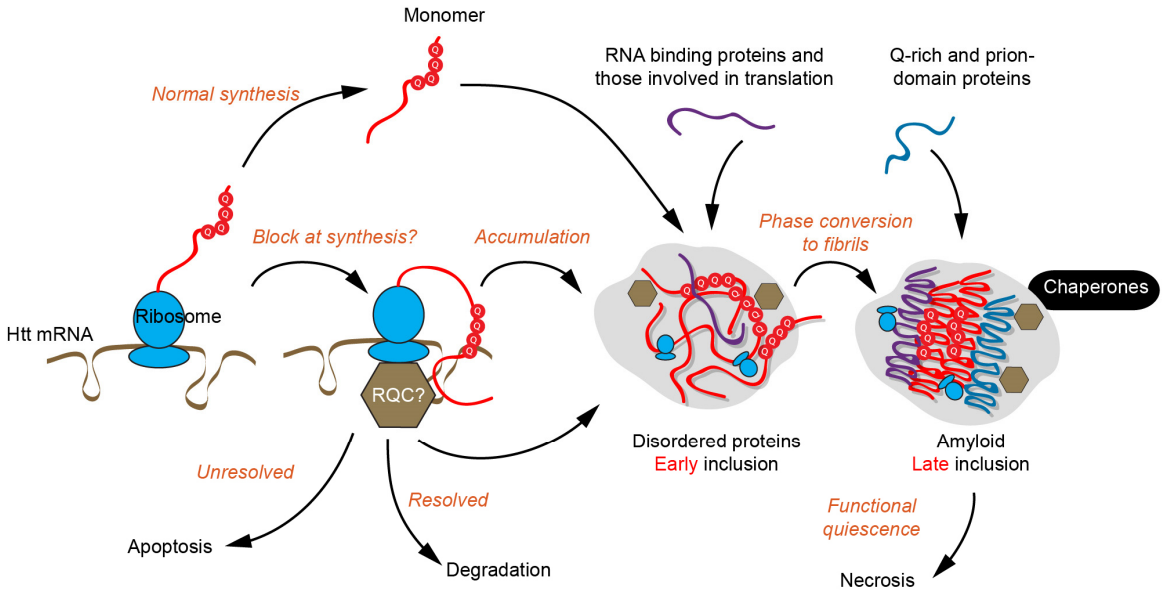

Figure S7: Model of soluble Httex1 toxicity, aggregation and progression to cellular quiescence (Relates to discussion section of manuscript). Soluble Httex1 confers toxicity via mitochondrial membrane hyperpolarization and elicits an elevated apoptosis response. This may arise by problems during translation of the expanded polyQ sequence. Over time, the inclusion is nucleated, which is initially comprised of disordered Htt. These inclusions contain proteins involved in translation and associated ribonucleoproteins, possibly including a ribosomal quality control complex or related mechanism (RQC). Over time the inclusion converts into an amyloid structure, which correlates with increased co-aggregation of other glutamine-enriched proteins and proteins with predicted prion domains, notably stress granule proteins. The formation of mature inclusions reduces the trigger for apoptosis from soluble Httex1 and at the same time leads the cell into a functionally quiescent state. A slower necrotic death ensues.

Additional related discussion of the model.

The toxicity of soluble Httex1 may arise as a result of misfolding or micro-aggregation onto the translational machinery. In the early inclusions, key translational machinery were enriched, including ribosome components, suggesting that the initial inclusions emerge from clusters of nascent Httex1-ribosome complexes, and may disrupt translation. Also enriched were ribonucleoproteins of which several (e.g. HNRNP family) have functions spanning translational regulation and other RNA processing functions (such as splicing, mRNA stability and ribosome biogenesis) (Geuens et al., 2016). This opens the possibility that the early steps of aggregation involving mRNA-ribosome-Httex1 complexes may ultimately sequester associated RNA processing machinery into the inclusion. Similar associations have been recently reported with soluble oligomeric Httex1 states preferentially binding to ribonucleoproteins (Kim et al., 2016).

As the Htt in the inclusions converted into amyloid, there was a correlating enrichment of RNA granule and prion domain predicted proteins as well as Httex1 itself. Low-complexity domains of FUS and HNRNP family for example (interactors of late inclusions) are able to form liquid droplet hydrogels and these hence might be attracted into the inclusions through a co-mixing mechanism as Httex1 reorganizes into an amyloid structure. Our model posits co-aggregation as a mechanism to functionally impair these proteins and hence underpin a broader cascade of functional paralysis for establishing quiescence and necrotic death.

SUPPLEMENTAL REFERENCES

Abramoff, M.D., Magelhaes, P.J., and Ram, S.J. (2004). Image Processing With ImageJ. Biophotonics International *11*, 36-42.

Arrasate, M., Mitra, S., Schweitzer, E.S., Segal, M.R., and Finkbeiner, S. (2004). Inclusion Body Formation Reduces Levels of Mutant Huntingtin and the Risk of Neuronal Death. Nature *431*, 805-810.

Bassan, P., Byrne, H.J., Lee, J., Bonnier, F., Clarke, C., Dumas, P., Gazi, E., Brown, M.D., Clarke, N.W., and Gardner, P. (2009). Reflection contributions to the dispersion artefact in FTIR spectra of single biological cells. Analyst *134*, 1171-1175.

Belmokhtar, C.A., Hillion, J., and Segal-Bendirdjian, E. (2001). Staurosporine induces apoptosis through both caspase-dependent and caspase-independent mechanisms. Oncogene *20*, 3354-3362.

Denham, M., Parish, C.L., Leaw, B., Wright, J., Reid, C.A., Petrou, S., Dottori, M., and Thompson, L.H. (2012). Neurons derived from human embryonic stem cells extend long-distance axonal projections through growth along host white matter tracts after intra-cerebral transplantation. Front Cell Neurosci *6*.

Geuens, T., Bouhy, D., and Timmerman, V. (2016). The hnRNP family: insights into their role in health and disease. Hum Genet *135*, 851-867.

Hande, K.R. (1998). Etoposide: four decades of development of a topoisomerase II inhibitor. Eur J Cancer *34*, 1514-1521.

Heraud, P., Caine, S., Campanale, N., Karnezis, T., McNaughton, D., Wood, B.R., Tobin, M.J., and Bernard, C.C.A. (2010). Early detection of the chemical changes occurring during the induction and prevention of autoimmune-mediated demyelination detected by FT-IR imaging. Neuroimage *49*, 1180-1189.

Hipp, M.S., Patel, C.N., Bersuker, K., Riley, B.E., Kaiser, S.E., Shaler, T.A., Brandeis, M., and Kopito, R.R. (2012). Indirect inhibition of 26S proteasome activity in a cellular model of Huntington's disease. J Cell Biol *196*, 573-587.

Kim, W., Bennett, E.J., Huttlin, E.L., Guo, A., Li, J., Possemato, A., Sowa, M.E., Rad, R., Rush, J., Comb, M.J*., et al.* (2011). Systematic and quantitative assessment of the ubiquitin-modified proteome. Mol Cell *44*, 325-340.

Kim, Y.E., Hosp, F., Frottin, F., Ge, H., Mann, M., Hayer-Hartl, M., and Hartl, F.U. (2016). Soluble Oligomers of PolyQ-Expanded Huntingtin Target a Multiplicity of Key Cellular Factors. Mol Cell *63*, 951-964.

Lancaster, A.K., Nutter-Upham, A., Lindquist, S., and King, O.D. (2014). PLAAC: a web and command-line application to identify proteins with prion-like amino acid composition. Bioinformatics *30*, 2501-2502.

Lois, C., Hong, E.J., Pease, S., Brown, E.J., and Baltimore, D. (2002). Germline transmission and tissue-specific expression of transgenes delivered by lentiviral vectors. Science *295*, 868-872.

Munro, K.L., Bambery, K.R., Carter, E.A., Puskar, L., Tobin, M.J., Wood, B.R., and Dillon, C.T. (2010). Synchrotron radiation infrared microspectroscopy of arsenic-induced changes to intracellular biomolecules in live leukemia cells. Vibrational Spectroscopy *53*, 39-44.

Olshina, M.A., Angley, L.M., Ramdzan, Y.M., Tang, J., Bailey, M.F., Hill, A.F., and Hatters, D.M. (2010). Tracking mutant huntingtin aggregation kinetics in cells reveals three major populations that include an invariant oligomer pool. J Biol Chem *285*, 21807-21816.

Ramdzan, Y.M., Nisbet, R.M., Miller, J., Finkbeiner, S., Hill, A.F., and Hatters, D.M. (2010). Conformation sensors that distinguish monomeric proteins from oligomers in live cells. Chem Biol *17*, 371-379.

Ramdzan, Y.M., Polling, S., Chia, C.P., Ng, I.H., Ormsby, A.R., Croft, N.P., Purcell, A.W., Bogoyevitch, M.A., Ng, D.C., Gleeson, P.A*., et al.* (2012). Tracking protein aggregation and mislocalization in cells with flow cytometry. Nat Methods *9*, 467-470.

Stewart, S.A., Dykxhoorn, D.M., Palliser, D., Mizuno, H., Yu, E.Y., An, D.S., Sabatini, D.M., Chen, I.S., Hahn, W.C., Sharp, P.A*., et al.* (2003). Lentivirus-delivered stable gene silencing by RNAi in primary cells. RNA *9*, 493-501.

Subach, F.V., Subach, O.M., Gundorov, I.S., Morozova, K.S., Piatkevich, K.D., Cuervo, A.M., and Verkhusha, V.V. (2009). Monomeric Fluorescent Timers that Change Color from Blue to Red Report on Cellular Trafficking. Nat Chem Biol *5*, 118-126.

Szklarczyk, D., Franceschini, A., Wyder, S., Forslund, K., Heller, D., Huerta-Cepas, J., Simonovic, M., Roth, A., Santos, A., Tsafou, K.P.*, et al.* (2015). STRING v10: protein-protein interaction networks, integrated over the tree of life. Nucleic Acids Res *43*, D447-452.

Tobin, M.J., Puskar, L., Barber, R.L., Harvey, E.C., Heraud, P., Wood, B.R., Bambery, K.R., Dillon, C.T., and Munro, K.L. (2010). FTIR spectroscopy of single live cells in aqueous media by synchrotron IR microscopy using microfabricated sample holders. Vibrational Spectroscopy *53*, 34-38.

Tsvetkov, A.S., Miller, J., Arrasate, M., Wong, J.S., Pleiss, M.A., and Finkbeiner, S. (2010). A small-molecule scaffold induces autophagy in primary neurons and protects against toxicity in a Huntington disease model. Proc Natl Acad Sc USA *107*, 16982-16987.

van Delft, M.F., Wei, A.H., Mason, K.D., Vandenberg, C.J., Chen, L., Czabotar, P.E., Willis, S.N., Scott, C.L., Day, C.L., Cory, S.*, et al.* (2006). The BH3 mimetic ABT-737 targets selective Bcl-2 proteins and efficiently induces apoptosis via Bak/Bax if Mcl-1 is neutralized. Cancer Cell *10*, 389-399.

Venzon, D.J., and Moolgavkar, S.H. (1988). A Method for Computing Profile-Likelihood-Based Confidence-Intervals. Applied Statistics-Journal of the Royal Statistical Society Series C *37*, 87-94.

Whelan, D.R., Bambery, K.R., Puskar, L., McNaughton, D., and Wood, B.R. (2013). Synchrotron Fourier transform infrared (FTIR) analysis of single living cells progressing through the cell cycle. Analyst *138*, 3891-3899.